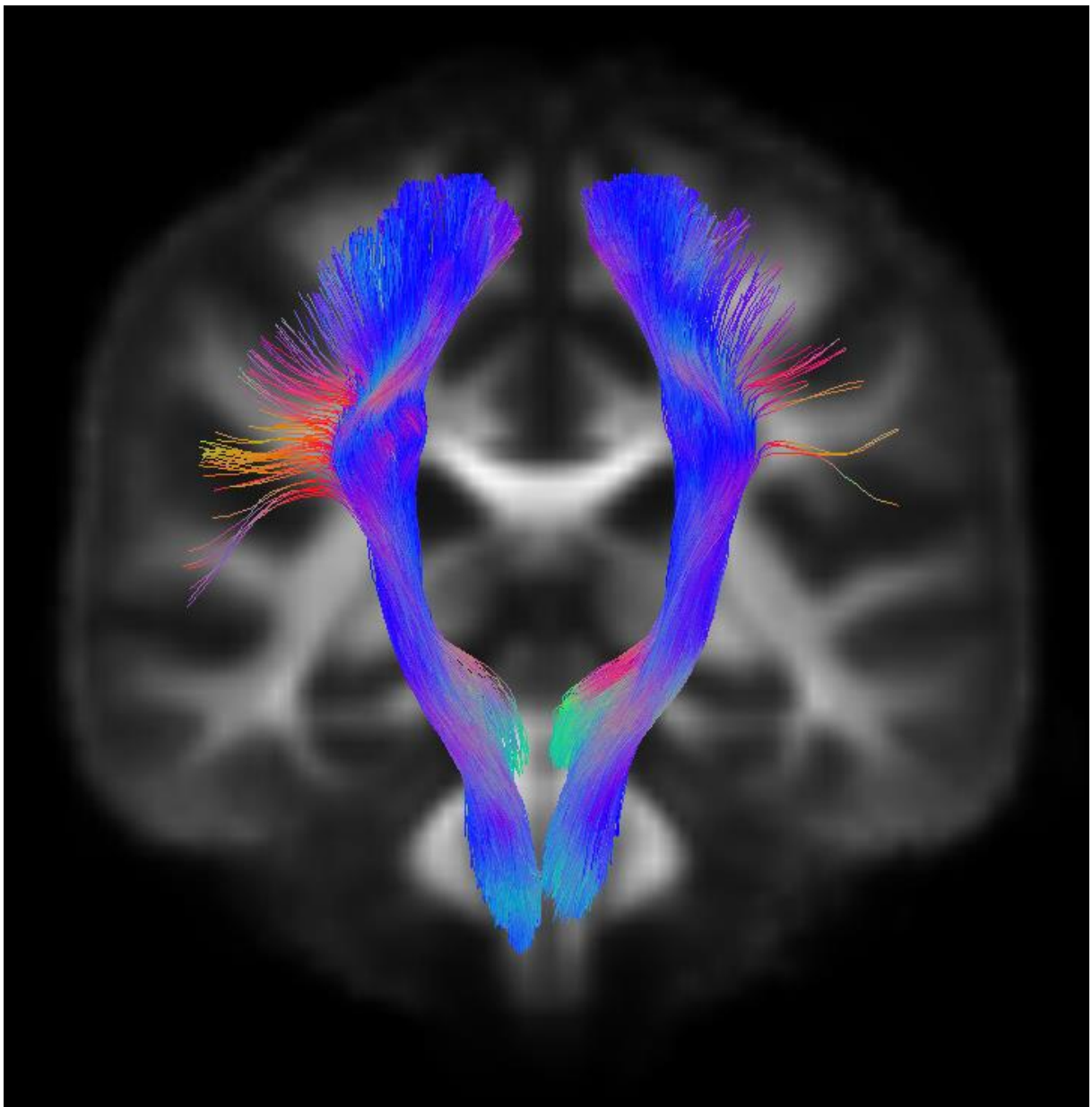


# White Matter Damage and Long-Term Neurological and Cognitive Outcome After Cardiac Arrest: A Clinical Tractography Study



**Nienke Gerards**

*A thesis submitted for the degree of Master of Science*

# White Matter Damage and Long-Term Neurological and Cognitive Outcome After Cardiac Arrest: A Clinical Tractography Study

**Nienke Rianne Gerards**

Enschede, January 18, 2023

University of Twente.

Technical Medicine – Medical Imaging and Intervention

Rijnstate, Arnhem

Department of Neurology and Clinical Neurophysiology

## **Examination committee**

Prof. dr. J. Hofmeijer	Chair & medical supervisor
Prof. dr. D.G. Norris	Technological supervisor
M.M.L.H Verhulst, MSc	Daily supervisor
Dr. M. Chamberland	Daily supervisor
Dr. M. Groenier	Process supervisor
Dr. ir. W.M. Brink	External member



## ABSTRACT

---

**Objectives** - Cerebral ischemia as a result of cardiac arrest may lead to changes in white matter structure, which can be detected by diffusion tensor imaging (DTI). Therefore, early measures obtained from DTI scans might yield long-term information for the prediction of neurological and cognitive outcome after cardiac arrest. Here, we study the associations between early diffusivity measures in five a priori selected white matter tracts and neurological outcome six months and cognitive performance twelve months after cardiac arrest.

**Methods** – We analysed DTI scans from two ongoing prospective cohort studies. Comatose patients with an MRI scan between 2-9 days were included in our analysis of neurological outcome. Patients that regained consciousness with an MRI scan between 2-30 days were included in our analysis of cognitive performance. Neurological outcome was assessed at six months, dichotomized as good (Cerebral Performance Category (CPC) 1-2) and poor (CPC 3-5). Cognitive performance was defined as either normal (Montreal Cognitive Assessment (MoCA)  $\geq 26$ ) or impaired (MoCA  $< 26$ ). We calculated the mean fractional anisotropy (FA), mean diffusivity (MD), and apparent fiber density (AFD) in five white matter tracts: the genu and body of the corpus callosum, the superior longitudinal fasciculus, the uncinate fasciculus, the cortico-spinal tract, and the thalamo-occipital tract. The measures were compared between patients with good and poor neurological outcome and with normal and impaired cognition. Furthermore, we exploratively compared the mean FA, MD, and AFD in 30 tracts throughout the whole brain. Finally, we compared these measures between the different MRI scanners that were used in our study.

**Results** – Mean FA, MD, and AFD in the five tracts measured within the first week after cardiac arrest were not associated with neurological outcome at six months (n=64; 24 with poor outcome) or cognitive performance at twelve months (n=40; 20 with impaired cognition). Exploratory analyses showed that the FA in the cortico-striatal tracts, thalamocortical tracts and cerebellar peduncles was significantly lower in patients with poor neurological outcome than patients with good outcome. No associations were found between the diffusivity measures in any tract and cognitive performance. Statistically significant inter-vendor differences were found in all three diffusivity measures.

**Conclusion** – Our analysis implicates that the FA in individual tracts holds the potential for outcome prediction of comatose patients after cardiac arrest. However, a pragmatic solution to inter-vendor differences should be found before clinical application can be considered.

# CONTENT

Abstract.....	3
List of Abbreviations .....	6
1 Introduction.....	1
2 Objectives.....	2
2.1 Primary Objective.....	2
2.2 Secondary Objectives .....	2
3 Methods .....	3
3.1 Study Design.....	3
3.2 Participants .....	3
3.3 MRI Data Acquisition .....	4
3.4 MRI Processing.....	4
3.4.1 Preprocessing .....	5
3.4.2 Tract Segmentation.....	5
3.4.3 Diffusivity Measures .....	6
3.4.4 Visualization of Average Group Measures .....	7
3.5 Inter-Vendor Differences .....	7
3.6 Statistical Analyses .....	8
3.7 Post Hoc Analyses.....	8
4 Results .....	9
4.1 Subjects.....	9
4.2 Associations Between Diffusivity Measures and Neurological Outcome.....	11
4.3 Associations Between Diffusivity Measures and Cognitive Performance .....	12
4.4 Secondary Analysis of Diffusivity Measures and Neurological Outcome .....	13
4.5 Secondary Analysis of Diffusivity Measures and Cognitive Performance.....	14
4.6 Visualization of Average Group Diffusivity Measures .....	14
4.7 Inter-Vendor Comparison.....	16
4.8 Post Hoc Analyses.....	16
5 Discussion .....	18
6 Conclusion .....	21
7 References.....	22
Appendix A. Overview Preprocessing and Processing Scripts .....	26
Appendix B. Background: Preprocessing of diffusion MRI .....	28

Appendix C. Selection of Tracts for the Primary Analysis.....	31
Appendix D. Median Diffusivity Measures per Tract Grouped by Cognitive Performance .....	33
Appendix E. Median Diffusivity Measures per Tract Grouped by Neurological Outcome in Rijnstate Population.....	34
Appendix F. Median Diffusivity Measures per Tract Grouped by Cognitive performance in Rijnstate Population.....	35

## LIST OF ABBREVIATIONS

---

<b>Abbreviation</b>	<b>Definition</b>
AFD	Apparent Fiber Density
CPC	Cerebral Performance Category
CSD	Constrained Spherical Deconvolution
CSF	Cerebral Spinal Fluid
DTI	Diffusion Tensor Imaging
DWI	Diffusion-Weighted Imaging
EPI	Echo Planar Imaging
FA	Fractional Anisotropy
fODF	fiber Orientation Distribution Function
MD	Mean Diffusivity
MoCA	Montreal Cognitive Assessment
MRI	Magnetic Resonance Imaging
Synb0-DISCO	Synthesized b0 diffusion distortion correction

# 1 INTRODUCTION

---

In the Netherlands, the incidence of out-of-hospital cardiac arrest is high with approximately 17.000 cases per year (1). Even though survival rates after cardiac arrest have increased over the last 40 years, around 50% of patients admitted to the Intensive Care Unit with post-anoxic coma do not survive (2-4). Survival is predominantly determined by neurological function, which is often affected by hypoxic-ischemic brain injury (5). Even among patients who have a seemingly good recovery, cognitive impairments remain persistent as a result of this brain injury (6). These long-term cognitive disturbances are reported among 42-50% of surviving patients, mostly affecting their memory, attention, and executive functioning (7-11). These impairments can impact a patient's daily functioning, often leading to a decreased quality of life and ability to socially participate (6, 8).

Accurate prognostication of good or poor neurological outcome in the comatose phase after cardiac arrest would contribute to decisions on continuing life-sustaining treatment and counselling of relatives. In patients with good neurological recovery, early recognition of long-term cognitive disturbances would allow for better guidance during rehabilitation and the development of new treatment strategies (12). Both prediction of neurological outcome and early recognition of long-term cognitive impairments require early biomarkers that yield long-term prognostic information.

To search for biomarkers, understanding the pathophysiological processes in the ischemic brain is important. At the onset of a cardiac arrest, cerebral blood flow approaches zero and remains decreased even after the return of spontaneous circulation (13). The lower perfusion levels cause an interruption of brain activity, inciting a cascade of injurious events (14). One of the known effects is ATP depletion, which leads to depolarisation of the cell membrane followed by cell swelling and reduction of extracellular volume within 2-5 days after cardiac arrest (14, 15). This intracellular oedema, also called cytotoxic oedema, mostly affects astrocytes in both grey and white matter (16).

In our current study, we focus on diffusion-weighted imaging (DWI), a form of magnetic resonance imaging (MRI) that measures the diffusion of water molecules. In white matter, diffusion is highly anisotropic as myelin and axons restrict diffusion perpendicular to the fiber bundles (17, 18). Therefore, modelling the diffusion-weighted signal can provide information about the microstructural organization of white matter (19, 20). Various models of the diffusion-weighted signal within a voxel are available, including the Diffusion Tensor Imaging (DTI) model and the fiber Orientation Distribution Function (fODF). The DTI model represents only one major fiber orientation within a voxel, while the fODF can represent multiple orientations. Two important measures derived from the DTI model are Fractional Anisotropy (FA) and Mean Diffusivity (MD), reflecting the directionality and magnitude of the diffusion signal (20). Apparent Fiber Density (AFD) is a metric obtained from the fODF and reflects white matter fiber density within a voxel (21).

Diffusivity measures are calculated for each voxel but hold more value for prediction in clinical practice when averaged over a larger region in the brain. Previous studies have mostly investigated mean diffusivity measures of the whole brain or whole-brain white matter (22, 23). However, we expect that measures calculated for individual white matter tracts might be more sensitive for differentiating between patients with good and poor neurological outcome and recognizing cognitive impairments early on, since certain tracts might be affected more by ischemia than others.

The FA is the only measure that has previously been studied in specific white matter regions in relation to neurological outcome in patients after cardiac arrest (24). In multiple regions throughout the brain, the FA was significantly lower in patients with poor neurological outcome compared to patients with good outcome. MRI scans in this study were obtained eleven days after cardiac arrest. We hypothesize that these differences in FA are already present after three days due to diffusion restriction caused by cytotoxic oedema. The magnitude of diffusivity has only been investigated in whole-brain white matter after cardiac arrest and does not appear to differ between patients with good and poor neurological outcome (22, 25, 26). Therefore, we also do not expect differences in tract-specific MD values. The AFD is a relatively new measure (21) that has not been investigated in populations after cardiac arrest. We expect that the ratio between intracellular and extracellular volume will be increased three days after cardiac arrest in patients with poor outcome, as cytotoxic oedema causes swelling of the axons within 2-5 days after cardiac arrest. Thus, our hypothesis is that the AFD might be higher in patients with poor neurological outcome after cardiac arrest.

Research on associations between diffusivity measures and cognitive performance is non-existent in cardiac arrest survivors. Studies in other populations, such as patients after traumatic brain injury do show correlations between tract-specific FA and MD and disturbances in memory, attention, and executive function (27, 28). We are curious to find out if cognitive performance is also associated with our diffusivity measures in patients after cardiac arrest.

To test our hypotheses, we analysed data from two ongoing prospective cohort studies in patients after cardiac arrest. We aimed to answer the following question: What are the associations between early diffusivity measures and long-term neurological outcome and cognitive performance after cardiac arrest? Primarily, we studied the FA, MD, and AFD in five a priori selected white matter tracts including the superior longitudinal fasciculus, the genu and body of the corpus callosum, the uncinate fasciculus, the corticospinal tract, and the thalamo-occipital tract. As a secondary explorative analysis, we investigated these measures in a larger set of white matter tracts throughout the whole brain.

## 2 OBJECTIVES

---

### 2.1 PRIMARY OBJECTIVE

The primary objective is to study the associations between early diffusivity measures in five a priori selected white matter tracts and (1) neurological outcome six months and (2) cognitive performance twelve months after cardiac arrest.

### 2.2 SECONDARY OBJECTIVES

Secondary objectives include:

- To explore associations between early diffusivity measures in a large set of white matter tracts throughout the whole brain and neurological outcome six months after cardiac arrest.
- To explore associations between early diffusivity measures in a large set of white matter tracts throughout the whole brain and cognitive performance twelve months after cardiac arrest.

## 3 METHODS

---

### 3.1 STUDY DESIGN

We analysed data from our two ongoing prospective multicentre cohort studies: the Cracking Coma study and the Brain Outcome After Cardiac Arrest (BROCA-)prediction study. The Cracking Coma study investigates neurological outcome prediction in comatose patients after cardiac arrest and the BROCA-prediction study focuses on the prediction of long-term cognitive impairments in cardiac arrest survivors. Both trials collected MRI data in three Dutch hospitals: Rijnstate hospital (Arnhem), Radboud university medical centre (Nijmegen), and Maastricht university medical centre (Maastricht). The Committee on Research Involving Human Subjects region Arnhem-Nijmegen approved both studies. For the current analysis, we used MRI data collected between June 2018 and February 2022.

### 3.2 PARTICIPANTS

Patients were included in the Cracking Coma study after permission from their legal representatives within 72 hours after cardiac arrest. The BROCA-prediction study included patients after informed consent was obtained from either the patient or their legal representative. The inclusion criteria for both studies are listed in Figure 1. Patients could be included in both studies as the inclusion criteria were not mutually exclusive. The exclusion criteria for both studies were identical: pregnancy, a life expectancy of fewer than 24 hours post-cardiac arrest, any known progressive brain illness, pre-existent dependency in daily living (Cerebral Performance Category (CPC) 3-4), or a contraindication to undergo MRI examination.

Patients included in the Cracking Coma study were eligible for our analysis of neurological outcome six months after cardiac arrest. The outcome measure for this analysis was “good” (CPC 1-2, no or moderate neurological disability) or “poor” (CPC 3-5, severe neurological disability, vegetative state, or death) neurological outcome at six months after cardiac arrest. For our analysis of cognitive performance twelve months after cardiac arrest, patients were eligible when they regained consciousness and were included in either the Cracking Coma or BROCA-prediction study. Cognitive performance was determined with the Montreal Cognitive Assessment (MoCA), an international and validated screening tool for the detection of mild cognitive impairments in cardiac arrest survivors in the following cognitive domains: executive functioning, visuospatial abilities, attention, concentration, working memory, language, abstract reasoning and orientation (29). The MoCA score ranges from 0 to 30. The outcome measure for our analysis of cognitive performance was cognitive performance twelve months after cardiac arrest, defined as impaired cognition (MoCA < 26) or normal cognition (MoCA ≥ 26).

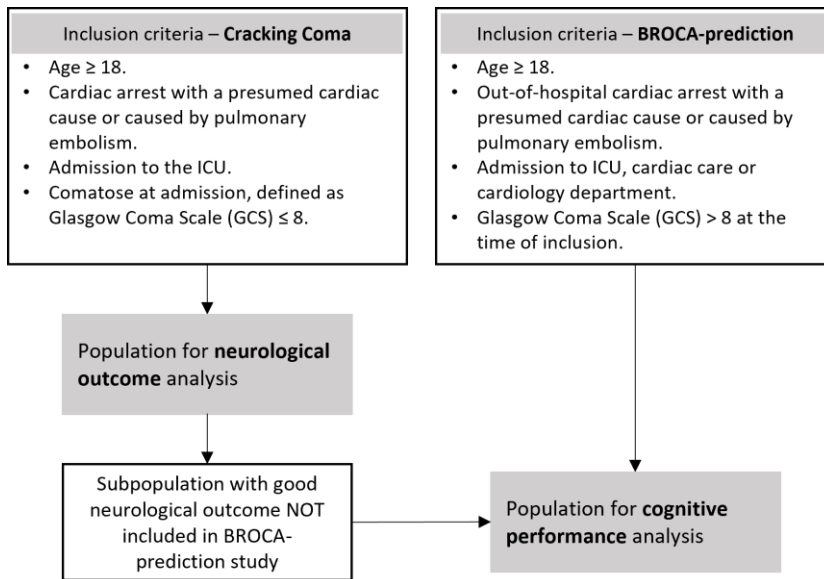


Figure 1: Inclusion criteria for patients in the Cracking Coma study and BROCA-prediction study and the subsequent eligibility for our analysis of neurological outcome at six months and cognitive performance at twelve months. Patients can be included in both studies and analyses. A small subgroup of patients from neurological outcome group was also eligible for the cognitive performance analysis without being included in the BROCA-prediction study. ICU = intensive care unit.

Table 1: MRI acquisition parameters for the T1 and DTI sequences of the Philips Ingenia and Siemens Skyra scanners.

Sequence characteristics	Philips Ingenia		Siemens Skyra	
	T1	DTI	T1	DTI
Repetition time (s)	8	9.0	2400	9.7
Echo time (ms)	3	95	3	95
Flip angle (degrees)	8	90	8	90
Voxel size (mm)	1 x 1 x 1	2 x 2 x 2	0.9 x 0.9 x 1	2 x 2 x 2
b-values (s/mm <sup>2</sup> )	-	b=0, b=1000	-	b=0, b=1000
Number of b=0 images	-	1	-	2*
Number of diffusion directions	-	30	-	32

\*The Siemens Skyra acquired two b<sub>0</sub>-scans and two times 32 diffusion scans with the same diffusion directions. Only the first b<sub>0</sub> and 32 diffusion scans were included in our analysis because of software limitations. T1 = T1 weighted, DTI = diffusion tensor imaging.

### 3.3 MRI DATA ACQUISITION

Magnetic resonance imaging (MRI) was acquired between 2 and 9 days after cardiac arrest for our neurological outcome analysis and between 2 and 30 days for our cognitive outcome analysis. The scans were acquired on two types of 3T scanners (Philips Ingenia [Rijnstate and Maastricht UMC+] or Siemens Skyra [Radboudumc]). The scanning protocol included T1 and DTI sequences and protocols were harmonized for the two types of scanners. Details of the sequences are listed in Table 1.

### 3.4 MRI PROCESSING

The MRI workflow included three steps: (I) preprocessing of the diffusion MRI scans, (II) white matter tractography, and (III) computation of diffusivity measures per white matter tract. These steps are described in detail in the following paragraphs. An overview of the scripts used to perform the workflow is given in Appendix A.

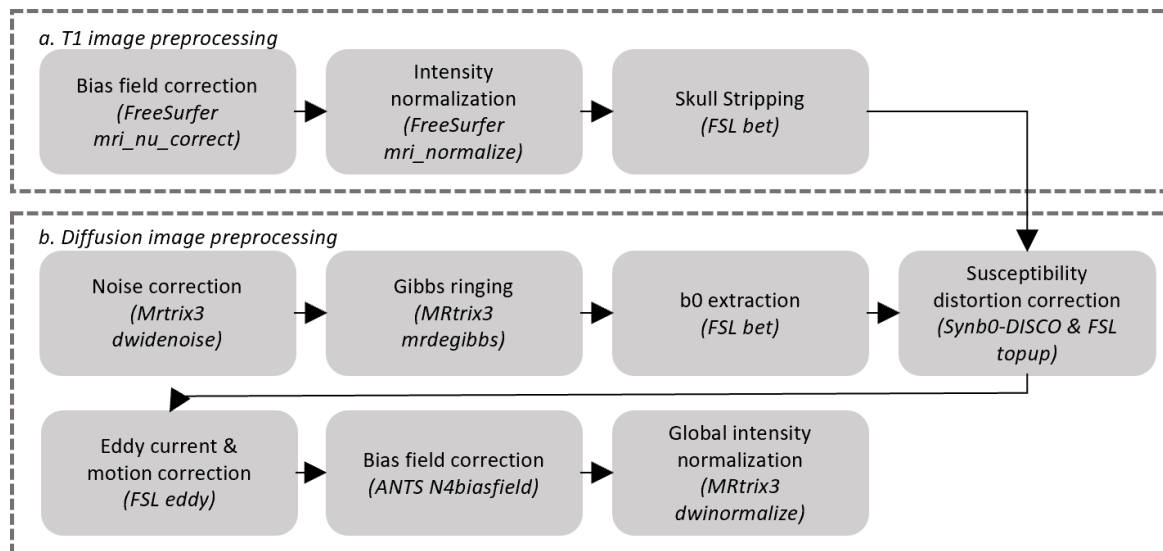


Figure 2: Workflow for preprocessing the diffusion and T1 MRI scans, including the software and specific functions used for each step.

### 3.4.1 Preprocessing

Our preprocessing pipeline is presented in Figure 2 and additional background information on diffusion MRI artefacts and preprocessing can be found in Appendix B. Our pipeline started with denoising and Gibbs unringing the diffusion images using MRtrix3 (30, 31). From the resulting image, the B0 image was extracted and used to create a brain mask with FSL (32) for skull-stripping the diffusion images. The T1 images were preprocessed with N3 bias field correction and intensity normalization, as implemented in FreeSurfer (33).

Because our diffusion MRI was acquired without reverse phase-encoding scans, the SynB0-DISCO technique (34) was used to synthesize an undistorted B0 image by registering the distorted B0 image to the preprocessed T1 image. The synthesized undistorted B0 image and the original distorted B0 image were used as input for topup (35) in FSL (36) to correct the diffusion images for susceptibility distortion correction. The eddy tool (37) in FSL was then used to correct for eddy currents and subject movement. After eddy, bias field inhomogeneities were corrected using N4 bias field correction in ANTS (38). Finally, we applied global intensity normalization, as implemented in MRtrix3, to further harmonize the data between our two scanners.

### 3.4.2 Tract Segmentation

The preprocessed diffusion data was submitted into TractSeg (39). TractSeg is a neural network-based approach that can segment 72 white matter tracts directly from the diffusion image. The reasons for choosing TractSeg as segmentation method are that the network has been trained on a dataset very similar to ours and the high accuracy and high speed compared to six other state-of-the-art segmentation methods (39, 40).

The segmentation pipeline of TractSeg, presented in Figure 3, is as follows (41). First, the diffusion images are transformed into MNI space. Second, fiber orientation distribution functions (fODF) are estimated using constrained spherical deconvolution. The peaks of the fODF are extracted, which represent the most likely orientation of fiber bundles in every voxel. Only the three largest peaks are used as input to the neural network since TractSeg assumes that a maximum of three fiber bundles can pass through a single voxel. TractSeg uses 2D neural networks in two stages. In the first stage, one

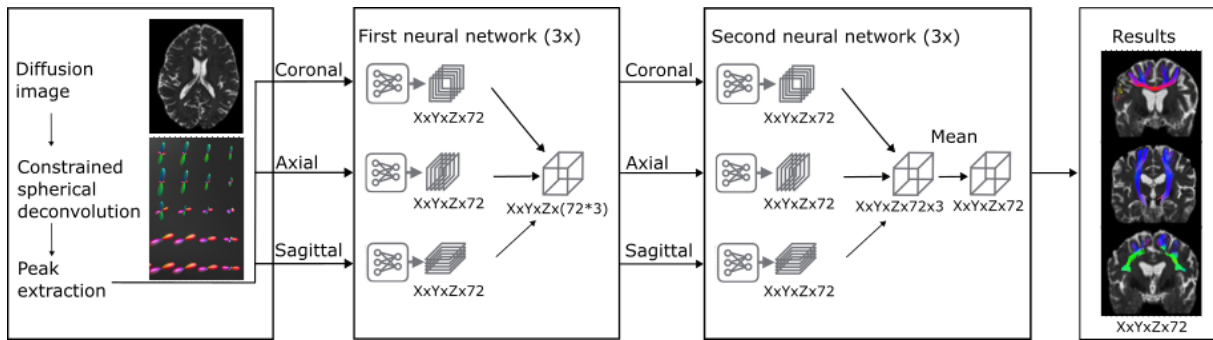


Figure 3: Segmentation pipeline of TractSeg. First box: The preprocessed diffusion image is used to calculate the fODF. The peaks of the fODF are extracted. Second box: The first neural networks segment fiber bundles per axis (coronal, axial, sagittal) using 2D information. Third box: The second neural networks learn the best combination of the three intermediate results to generate the final segmentation. Fourth box: 72 tracts are generated. Figure reproduced from *Wasserthal et al. (39)*

network per axis (coronal, axial, sagittal) is trained to segment the fiber bundles using only 2D information. In the second stage, the best combination of the three intermediate results is learned to generate the final segmentation of the 72 tracts.

For our primary analysis, we selected five tracts based on two requirements: (1) the tract was likely to be affected in patients with poor neurological outcome based on literature concerning diffusion tensor imaging in cardiac arrest patients, or (2) the tract correlated with cognitive impairments in patients with different neurological pathologies according to the literature. An overview of the available literature and the reasons for our selection can be found in Appendix C. The five tracts that we chose were the combined genu and body of the corpus callosum, the superior longitudinal fasciculus (SLF I, II and III combined), the uncinate fasciculus, the corticospinal tract, and the thalamo-occipital tract. For the tracts that existed in both hemispheres, we combined the left and right bundles into one tract since we expected brain damage in our population to be symmetric. The remaining tracts that were reconstructed by TractSeg were investigated in our explorative secondary analysis. Again, the same tracts in the left and right hemispheres were combined, resulting in a total of 30 tracts for our secondary analysis. An overview of the tracts can be found in Table 3 (1<sup>st</sup> column).

### 3.4.3 Diffusivity Measures

The diffusivity measures we derived from the data were the fractional anisotropy (FA), mean diffusivity (MD) and apparent fiber density (AFD). The FA and MD were derived from the diffusion tensor model, which represents the major fiber orientation within a voxel (42). For computation of the FA and MD maps, we used the Scilpy dMRI processing toolbox (43).

To calculate the AFD, we used a different diffusion model named constrained spherical deconvolution (CSD). CSD can model multiple fiber orientations within a voxel, which can be visualized using the fiber orientation distribution function (fODF). To compute the fODF, the average response functions for white matter and cerebral spinal fluid were calculated. The average response function of white matter described the diffusion-weighted signal from a single white matter fiber bundle in our population. Assuming that all white matter fiber bundles in the brain have identical diffusion characteristics, the diffusion-weighted signal can be described as the spherical convolution of the average response function with the fODF (Fig. 4). Thus, by reversing this process and computing the spherical

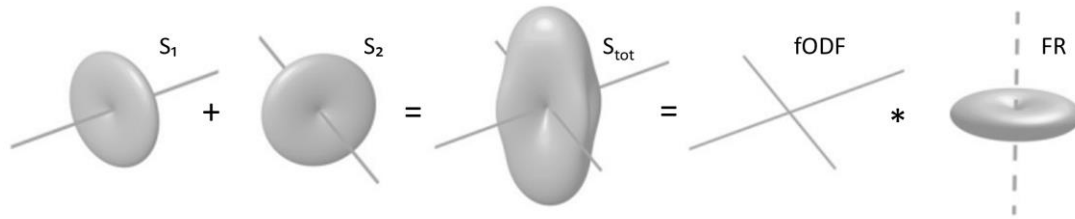


Figure 4: The spherical deconvolution approach. The total diffusion signal ( $S_{tot}$ ) is an addition of signals from multiple single fiber populations ( $S_1$ ,  $S_2$ ). The fiber orientation distribution function (fODF) is therefore equivalent to the spherical deconvolution of the total signal and the fiber response function (FR). Figure reproduced from *Dell'Aqua et al. (45)*

deconvolution of the response function from the diffusion-weighted signal, we obtained the fODF in each voxel. (44, 45) The AFD was calculated by taking the mean of the fODF per voxel.

The FA, MD, and AFD maps were transformed from subject space to MNI space with a rigid body transformation using the transform matrix previously determined by TractSeg. Mean FA, MD and AFD values per tract were computed by sampling the value of the maps at each point along each streamline using MRtrix3 and averaging the values obtained from the streamlines in one tract.

#### 3.4.4 Visualization of Average Group Measures

To visually compare the diffusivity measures within a tract between groups instead of individual patients, individual FA maps were again registered to standard space (FMRIB58\_FA), but this time with a non-linear transformation using the FSL function FNIRT. MD and AFD maps were also registered using the subject-specific transformations obtained with the FA maps. Afterwards, the individual maps in standard space were averaged for patients with good and poor neurological outcome with MRtrix3 (46). The average maps of patients with good outcome were subtracted from the average maps of patients with poor neurological outcome and vice versa. This resulted in two final maps per measure showing the difference between patients with good and poor neurological outcome. These maps were solely used for visualization and not for any statistical testing.

### 3.5 INTER-VENDOR DIFFERENCES

Inter-vendor reliability is a prominent issue given that we used MRI scanners from two different vendors (Philips and Siemens). To assess the effect of acquiring our data with two different scanners on our diffusivity measures, we compared mean whole-brain white matter FA, MD, and AFD values between patients whose scan was acquired on the Philips Ingenia and patients scanned with the Siemens Skyra. This analysis was performed in our neurological outcome analysis population. We obtained a patient-specific white matter mask by first registering the T1 image to the FA map using the FSL function flirt (47, 48) followed by segmentation of the registered image into different tissue types with the function *fast* (49) in FSL. After visual inspection, the white matter mask was eroded by one voxel. This was to ensure that the mask only included white matter because it would be better to miss the edges of white matter than to include voxels containing grey matter or cerebral spinal fluid with completely different diffusion properties. Mean FA, MD, and AFD values were calculated within the whole-brain white matter mask and compared between vendors.

### 3.6 STATISTICAL ANALYSES

Statistical analyses were performed in MATLAB R2021b. Assumptions of normality and homogeneity of variances were assessed by inspection of the Q-Q plots, histograms and Levene's test. Normally distributed variables were expressed as mean  $\pm$  SD and non-normally distributed variables as median [25<sup>th</sup>, 75<sup>th</sup> interquartile range]. Patients with good neurological outcome (CPC 1-2) were compared with patients with poor neurological outcome (CPC 3-5). Patients with normal cognition at 12 months (MoCA $\geq$ 26) were compared with patients with impaired cognition at 12 months (MoCA<26). Continuous variables were compared using the independent t-test or the Mann-Whitney U test depending on the distribution of the variables. Categorical variables were compared using the Chi-squared test. The false discovery rate according to the Benjamini-Hochberg procedure (50) was used to correct for multiple comparisons in our primary analysis. Our secondary explorative analyses and post hoc analyses were not corrected for multiple comparisons.

### 3.7 POST HOC ANALYSES

We performed two post hoc analyses. In the first post hoc analysis, the effect of inter-vendor differences was removed by including only patients scanned with the Philips Ingenia scanner at the Rijnstate hospital. Within this subset, we reinvestigated the associations between our diffusivity measures and neurological outcome and cognitive performance in all white matter tracts.

For the second post hoc analysis, we compared mean whole-brain white matter FA, MD, and AFD between patients with good and poor neurological outcome and between patients with normal and impaired cognition. This analysis was added to be able to compare our diffusivity results with previous studies because whole-brain white matter is investigated more frequently than individual tracts.

## 4 RESULTS

### 4.1 SUBJECTS

We screened 89 patients with an MRI within 30 days after resuscitation for eligibility and included 78 patients as visualized in the flow chart in Figure 5. Reasons for exclusion were the absence of the diffusion or T1 scan (n=5) or problems with the (pre)processing of scans (n=5). One patient was excluded because of missing volumes in the DTI scan. Of the remaining 78 patients, 64 were included in our neurological outcome analysis, and 40 were included in our cognitive performance analysis. Ten patients were included in both analyses.

The baseline characteristics of the neurological outcome group and the cognitive performance group are listed in Table 2. In our neurological outcome population, there were significant differences between patients with good and poor neurological outcome in age, sex, time to return of spontaneous circulation, and whether a patient was comatose during the MRI scan or not. In our cognitive performance population, significant differences between patients with cognitive impairments and patients without cognitive impairments were only seen in the time between cardiac arrest and the MRI scan.

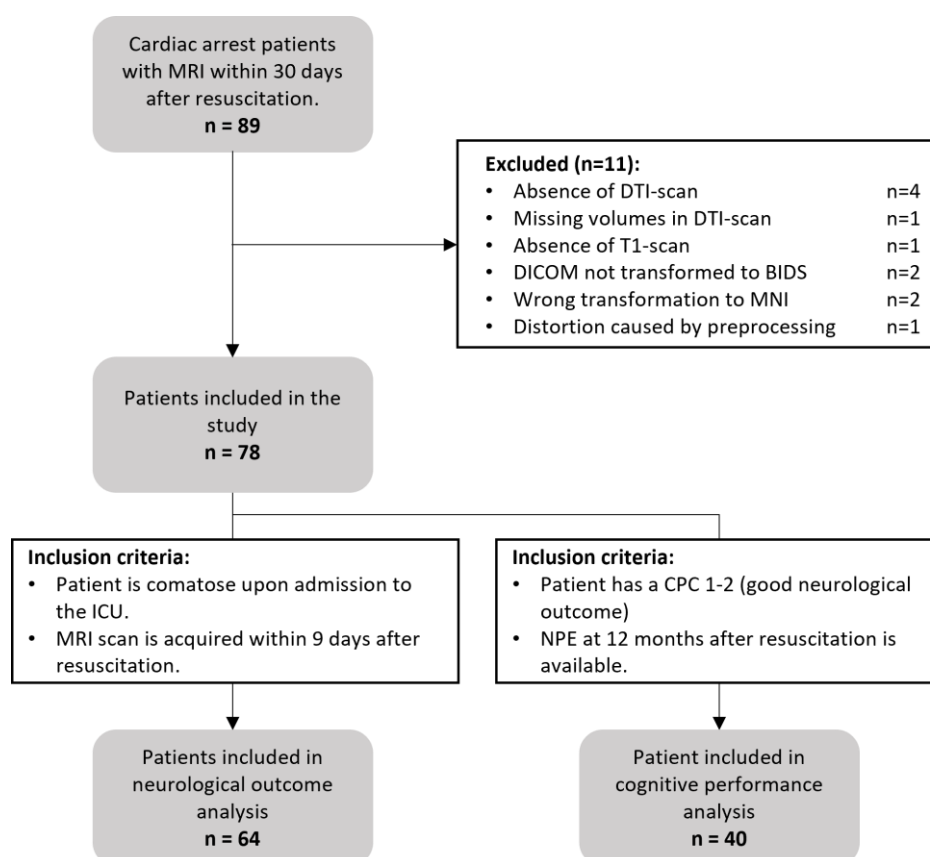


Figure 5: Flow chart of patient selection. Ten patients were included in both the neurological outcome analysis and the cognitive performance analysis. DTI = diffusion tensor imaging, ICU = Intensive Care Unit, CPC = Cerebral Performance Category, NPE = neurophysiological exam.

Table 2: Baseline characteristics of the patients with good and poor neurological outcome six months after cardiac arrest and of the patients with normal cognition and impaired cognition twelve months after cardiac arrest.

<b>Variable</b>	<b>Good neurological outcome (n=40)</b>	<b>Poor neurological outcome (n=24)</b>	<b>p-value</b>
Male	34 (85)	15 (63)	0.04*
Age	58 [49.25 – 65.00]	69.50 [57.00 – 74.00]	<0.01*
Time to ROSC (min)	12.50 [10.00 – 15.00]	21.50 [15.75 – 33.75]	<0.01*
Time between CA and MRI (days)	3.24 [2.37 – 4.15]	3.19 [2.36 – 3.92]	0.57
Comatose during MRI	26 (65)	23 (96)	<0.01*
<i>Scanner type</i>			
Philips	28 (70)	20 (83)	0.23
Siemens	12 (30)	4 (17)	
<i>Initial rhythm</i>			
Ventricular fibrillation	33 (82)	13 (54)	<0.01*
Asystole	-	5 (21)	
Unknown	7 (18)	6 (25)	
<i>CPC-score at six months</i>			
CPC 1	21 (53)	-	-
CPC 2	19 (46)	-	
CPC 3	-	4 (17)	
CPC 4	-	-	
CPC 5	-	20 (83)	
<b>Variable</b>	<b>Normal cognition (n=20)</b>	<b>Impaired cognition (n=20)</b>	<b>p-value</b>
Male	18 (90)	16 (80)	0.38
Age	59 [50.50 – 64.25]	60 [51.75 – 67.50]	0.54
Time to ROSC (min)	10 [7.50 – 15.00]	12 [9.25 – 19.50]	0.47
Time between CA and MRI (days)	3.59 [2.25 – 4.11]	5.05 [2.93 – 9.93]	0.05*
Comatose at admission	19 (95)	19 (95)	1.00
Comatose during MRI	3 (15)	7 (35)	0.14
MoCA score at 12 months	28.50 [27 – 29]	24 [22 – 25]	<0.01*
<i>Scanner type</i>			
Philips	15 (75)	17 (85)	0.43
Siemens	5 (25)	3 (15)	
<i>Initial rhythm</i>			
Ventricular fibrillation	18 (90)	15 (75)	-
Pulseless ventricular tachycardia	1 (5)	-	
Asystole	-	1 (5)	
Unknown	1 (5)	4 (20)	

Dichotomous variables are listed as n (%). Continuous variables are listed as median [IQR]. Group differences are calculated using Mann-Whitney U or chi-square tests. Significant differences are indicated by \*. ROSC = return of spontaneous circulation, CA = cardiac arrest, CPC = Cerebral Performance Category, MoCA = Montreal Cognitive Assessment.

## 4.2 ASSOCIATIONS BETWEEN DIFFUSIVITY MEASURES AND NEUROLOGICAL OUTCOME

The visual quality check showed that the five reconstructed white matter tracts were positioned at the correct location in the brain without any large inaccuracies (upper panel of Fig. 6). Median FA, MD, and AFD did not differ significantly between patients with good and poor neurological outcome in any of the five tracts (Fig. 6). The range of the MD and AFD was larger in patients with poor neurological outcome than patients with good outcome in all five tracts.

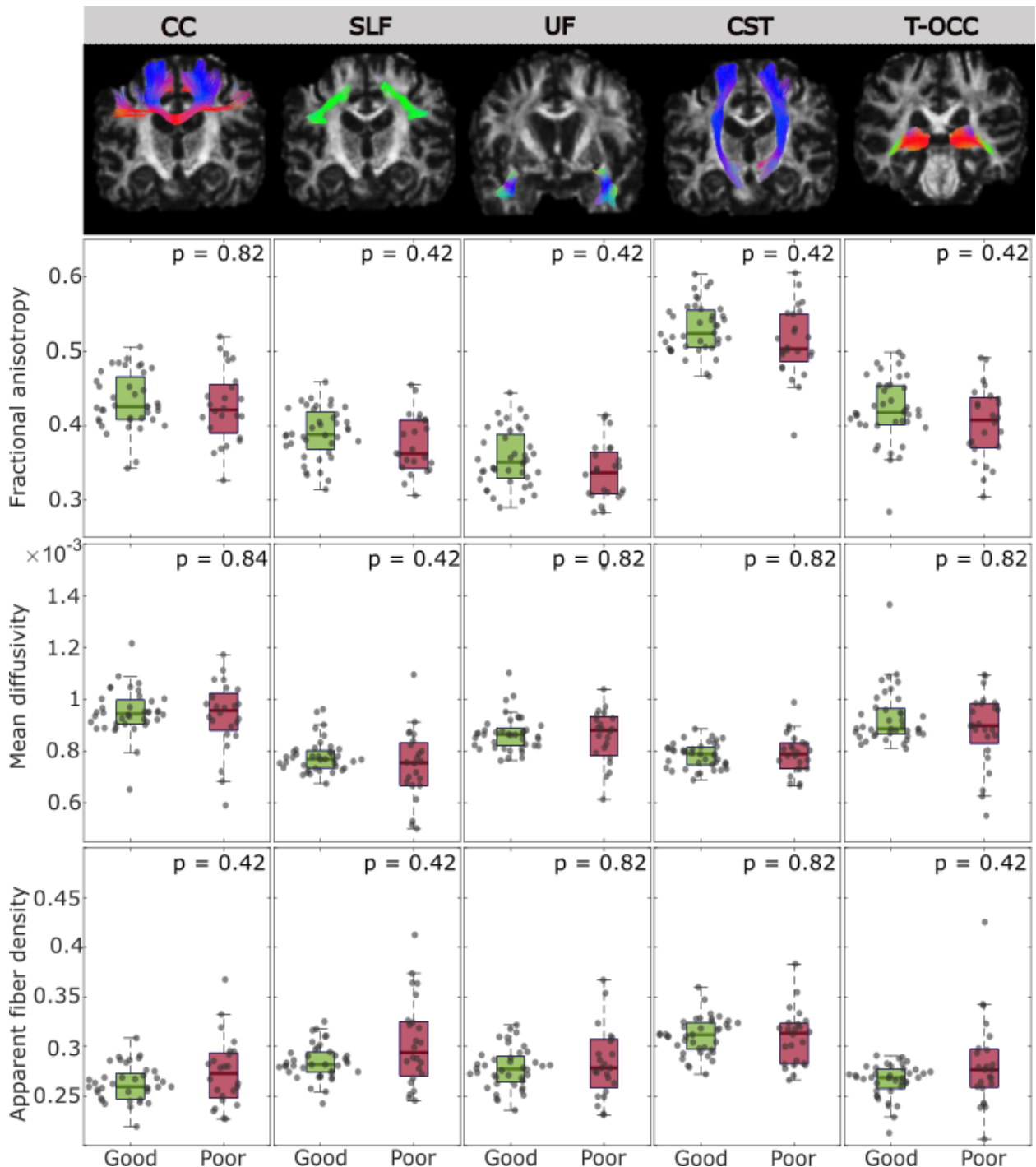


Figure 6: Visualization of the five preselected white matter tracts in a coronal slice in one patient and boxplots with the median FA, MD, and AFD values, grouped by neurological outcome (good or poor). P-values are corrected for multiple comparisons. CC = the genu and body of the corpus callosum, SLF = superior longitudinal fasciculus, UF = uncinate fasciculus, CST = corticospinal tract, T-OCC thalamo-occipital tract.

### 4.3 ASSOCIATIONS BETWEEN DIFFUSIVITY MEASURES AND COGNITIVE PERFORMANCE

We found no significant differences in FA, MD, and AFD between patients with impaired cognition and patients with normal cognition the five tracts (Fig. 7).

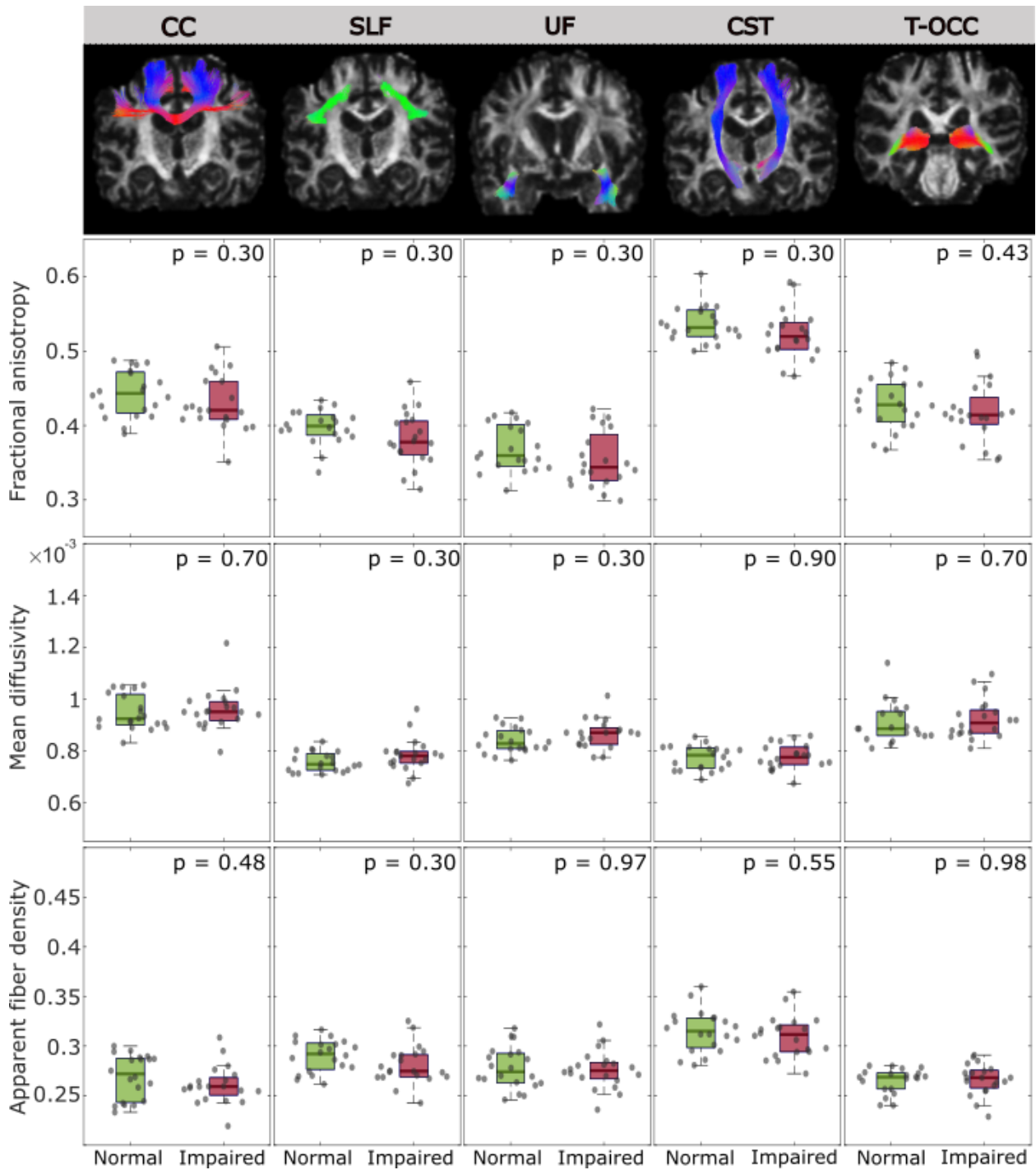


Figure 7: Visualization of the five preselected white matter tracts in a coronal slice in one patient and boxplots with the mean FA, MD and AFD values, grouped by cognitive performance (normal or impaired). P-values are corrected for multiple comparisons. CC = the genu and body of the corpus callosum, SLF = superior longitudinal fasciculus, UF = uncinate fasciculus, CST = corticospinal tract, T-OCC = thalamo-occipital tract.

Table 3: Median [IQR] fractional anisotropy, mean diffusivity, and apparent fiber density in 28 white matter tracts throughout the whole brain, grouped by neurological outcome (good or poor).

Metric	Fractional Anisotropy		Mean Diffusivity (*10 <sup>-3</sup> )		Apparent fiber density	
	Good (n=40)	Poor (n=24)	Good (n=40)	Poor (n=24)	Good (n=40)	Poor (n=24)
Arcuate fascicle	0.40 [0.38-0.41]	0.38 [0.36-0.40]	0.76 [0.73-0.78]	0.78 [0.76-0.81]	0.29 [0.28-0.30]	0.28 [0.27-0.29]
Anterior thalamic radiation	0.37 [0.34-0.38]	0.34 [0.32-0.38]	0.84 [0.81-0.89]	0.87 [0.85-0.89]	0.27 [0.25-0.28]	0.25 [0.25-0.26]
Commissure anterior	0.31 [0.27-0.37]	0.30 [0.25-0.37]	0.87 [0.83-0.97]	0.91 [0.82-0.95]	0.22 [0.20-0.24]	0.21 [0.17-0.23]
Rostrum (Corpus Callosum)	0.44 [0.41-0.48]	0.42 [0.38-0.45]	0.89 [0.84-0.94]	0.90 [0.88-0.96]	0.25 [0.23-0.27]	0.23 [0.23-0.24]
Isthmus (Corpus Callosum)	0.47 [0.44-0.50]	0.46 [0.43-0.49]	0.92 [0.89-0.97]	0.95 [0.90-1.00]	0.27 [0.26-0.28]	0.27 [0.26-0.28]
Splenium (Corpus Callosum)	0.51 [0.48-0.53]	0.49 [0.46-0.51]	1.01 [0.96-1.06]	1.02 [0.99-1.07]	0.27 [0.26-0.28]	0.27 [0.26-0.29]
Cingulum	0.40 [0.39-0.42]	0.38 [0.36-0.41]	0.77 [0.75-0.81]	0.80 [0.77-0.82]	0.29 [0.27-0.29]	0.28 [0.27-0.29]
Fronto-pontine tract	0.48 [0.46-0.51]	0.46 [0.43-0.48]	0.79 [0.74-0.81]	0.79 [0.76-0.82]	0.29 [0.27-0.31]	0.28 [0.27-0.30]
Inferior occipito-frontal fascicle	0.42 [0.40-0.44]	0.40 [0.39-0.42]	0.87 [0.83-0.93]	0.89 [0.86-0.93]	0.28 [0.26-0.28]	0.27 [0.26-0.28]
Inferior longitudinal fasciculus	0.42 [0.40-0.45]	0.41 [0.39-0.42]	0.84 [0.81-0.88]	0.87 [0.85-0.90]	0.26 [0.26-0.28]	0.27 [0.26-0.28]
Middle cerebellar peduncle	0.49 [0.47-0.50]	0.47 [0.46-0.50]	0.79 [0.74-0.81]	0.77 [0.74-0.83]	0.31 [0.29-0.32]	0.31 [0.29-0.34]
Middle longitudinal fasciculus	0.38 [0.36-0.41]	0.37 [0.35-0.40]	0.82 [0.79-0.85]	0.85 [0.81-0.86]	0.28 [0.27-0.29]	0.27 [0.27-0.28]
Optic radiation	0.43 [0.41-0.46]	0.42 [0.41-0.44]	0.88 [0.85-0.94]	0.89 [0.86-0.94]	0.27 [0.26-0.27]	0.27 [0.26-0.28]
Parieto-occipital pontine	0.48 [0.46-0.49]	0.46 [0.44-0.49]	0.84 [0.80-0.87]	0.85 [0.81-0.86]	0.29 [0.28-0.30]	0.29 [0.28-0.30]
Superior cerebellar peduncle	0.45 [0.44-0.47]	0.42 [0.41-0.47]	0.86 [0.84-0.91]	0.87 [0.85-0.95]	0.29 [0.28-0.31]	0.30 [0.28-0.31]
Striato-fronto-orbital tract	0.35 [0.33-0.38]	0.33 [0.30-0.36]	0.84 [0.80-0.89]	0.86 [0.84-0.88]	0.26 [0.24-0.28]	0.24 [0.24-0.26]
Striato-occipital tract	0.44 [0.42-0.45]	0.43 [0.41-0.45]	0.87 [0.84-0.91]	0.89 [0.86-0.95]	0.28 [0.27-0.28]	0.27 [0.27-0.29]
Striato-parietal tract	0.41 [0.39-0.42]	0.39 [0.37-0.42]	0.82 [0.79-0.85]	0.85 [0.81-0.85]	0.28 [0.27-0.29]	0.28 [0.27-0.28]
Striato-postcentral tract	0.41 [0.38-0.42]	0.39 [0.37-0.41]	0.77 [0.76-0.82]	0.81 [0.78-0.83]	0.29 [0.28-0.29]	0.28 [0.27-0.29]
Striato-precentral tract	0.41 [0.38-0.42]	0.39 [0.37-0.41]	0.75 [0.74-0.80]	0.79 [0.76-0.81]	0.30 [0.28-0.31]	0.28 [0.27-0.30]
Striato-prefrontal tract	0.32 [0.30-0.35]	0.35 [0.32-0.38]	0.85 [0.77-0.92]	0.84 [0.80-0.87]	0.28 [0.24-0.30]	0.26 [0.25-0.28]
Striato-premotor tract	0.33 [0.30-0.36]	0.35 [0.30-0.36]	0.77 [0.73-0.86]	0.78 [0.74-0.83]	0.29 [0.26-0.31]	0.27 [0.26-0.29]
Superior thalamic radiation	0.41 [0.39-0.46]	0.43 [0.41-0.46]	0.76 [0.70-0.82]	0.76 [0.73-0.78]	0.31 [0.28-0.33]	0.30 [0.29-0.31]
Thalamo-parietal tract	0.39 [0.36-0.43]	0.41 [0.38-0.45]	0.84 [0.78-0.90]	0.84 [0.82-0.88]	0.29 [0.27-0.31]	0.28 [0.27-0.29]
Thalamo-postcentral tract	0.42 [0.40-0.46]	0.44 [0.41-0.48]	0.77 [0.71-0.82]	0.78 [0.76-0.81]	0.31 [0.29-0.33]	0.30 [0.29-0.31]
Thalamo-precentral tract	0.41 [0.38-0.45]	0.43 [0.41-0.46]	0.75 [0.69-0.80]	0.76 [0.73-0.77]	0.32 [0.29-0.33]	0.30 [0.29-0.31]
Thalamo-prefrontal tract	0.35 [0.32-0.39]	0.38 [0.35-0.41]	0.86 [0.77-0.92]	0.83 [0.81-0.85]	0.28 [0.25-0.29]	0.27 [0.26-0.28]
Thalamo-premotor tract	0.36 [0.34-0.40]	0.39 [0.37-0.42]	0.80 [0.72-0.84]	0.77 [0.74-0.80]	0.29 [0.27-0.31]	0.28 [0.27-0.29]

Variables are listed as median [IQR]. P-values are without correction for multiple comparisons. Green boxes show a significant difference between patients with good and poor neurological outcome. Light green indicates a p-value <0.05 and dark green a p-value <0.01.

#### 4.4 SECONDARY ANALYSIS OF DIFFUSIVITY MEASURES AND NEUROLOGICAL OUTCOME

We included 28 out of 30 tracts reconstructed by TractSeg in our secondary analysis of neurological outcome. The reconstruction of the fornix was missing in three patients, because the small size of the fornix relative to the limited resolution of the underlying image hampered the reconstruction. The inferior cerebral peduncle could not be reconstructed by TractSeg in four patients, due to the tract being partially outside the field of view. Because we could not guarantee that the fornix and cerebellar peduncle were reconstructed correctly in the remaining patients, we excluded both tracts from our analysis.

Median FA, MD, and AFD values in the remaining white matter tracts are presented in Table 3. The FA was significantly lower in patients with poor neurological outcome compared to patients with good neurological outcome in seventeen tracts, including all cortico-striatal tracts, the cerebellar peduncles and most thalamocortical tracts. The AFD was significantly lower in patients with poor neurological outcome compared with patients with poor neurological outcome in the cingulum and striato-parietal tract.

## 4.5 SECONDARY ANALYSIS OF DIFFUSIVITY MEASURES AND COGNITIVE PERFORMANCE

The fornix and inferior cerebral peduncle were excluded from our secondary analysis of cognitive performance for the same reasons that they were excluded from the secondary analysis of neurological outcome. The FA and MD did not differ between patients with impaired cognition and patients with normal cognition in any of the twenty-eight tracts. The AFD was significantly lower in patients with impaired cognition compared to patients with normal cognition in the arcuate fascicle. Appendix D shows the median FA, MD and AFD for all twenty-eight tracts, grouped by cognitive performance.

## 4.6 VISUALIZATION OF AVERAGE GROUP DIFFUSIVITY MEASURES

Six subjects (four with poor outcome) were excluded from the averaged group maps, because the diffusion scans deviated too much from standard anatomy. These included three patients with large ventricles, which hampered the registration to standard space. In the other patients, the upper part of the brain was cut from the image due to poor placement of the field of view during acquisition.

Figure 8 shows the average FA, MD, and AFD maps of patients with good and poor neurological outcome, subtracted from each other and mapped over the five white matter tracts from our primary analysis. The subtracted maps show that the differences in FA vary greatly within all tracts. In some regions, the FA is higher in patients with good neurological outcome than in patients with poor outcome. Other regions, however, show the opposite effect or no difference. The differences in MD are more uniform within the tracts. Only in the cortical fiber endings, the MD is slightly lower in patients with poor neurological outcome. The AFD in the cortical fiber endings is higher in patients with poor neurological outcome, but not in other regions. Only in the uncinatus fasciculus, does the AFD appear to be higher in patients with poor neurological outcome throughout the whole tract.

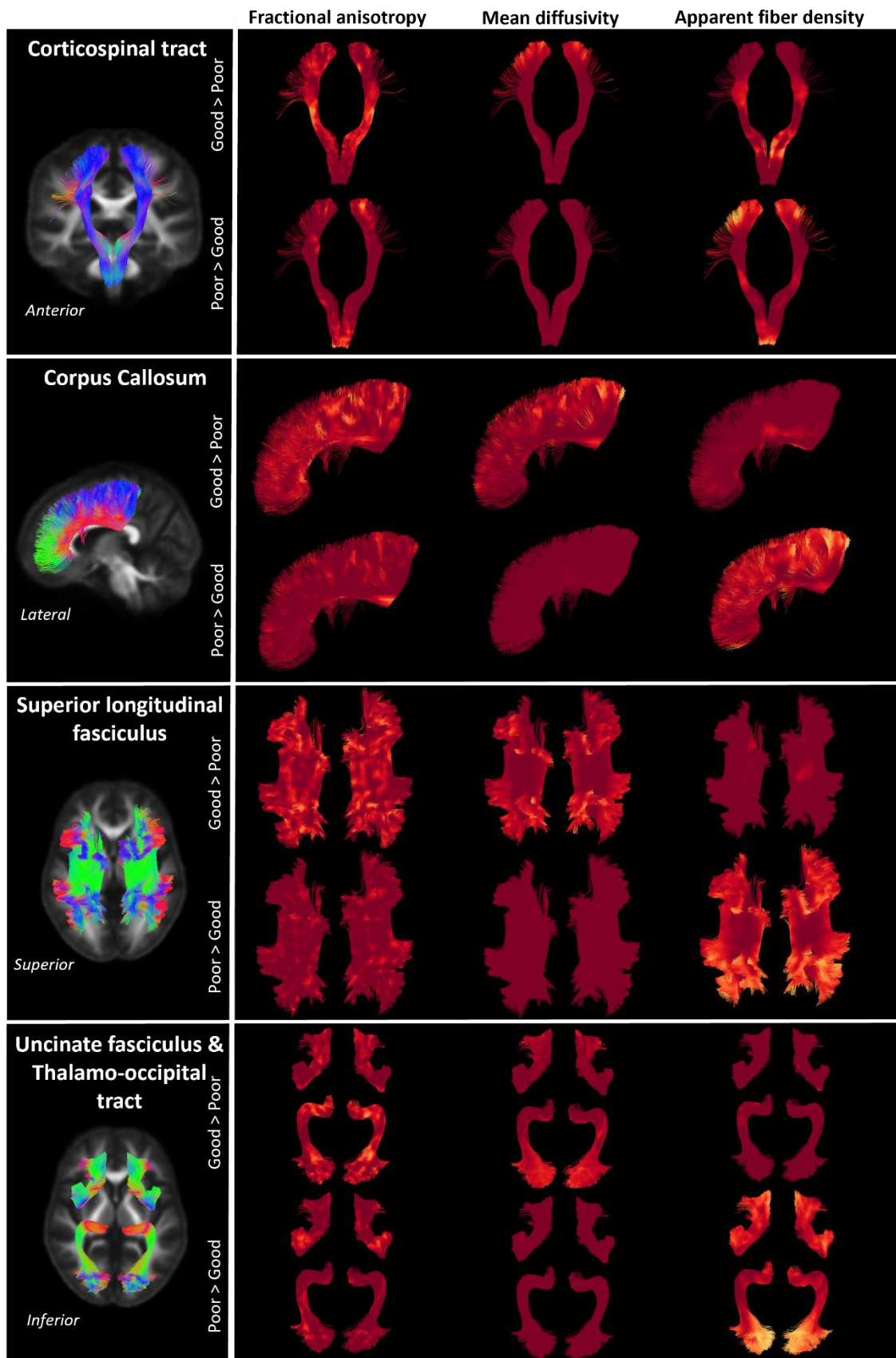


Figure 8: Average fractional anisotropy, mean diffusivity, and apparent fiber density for patients with good and poor neurological outcome subtracted from each other and mapped over the five white matter tracts. For each tract, the upper map shows where the diffusivity measure is larger in patients with good neurological outcome, while the lower map shows where the diffusivity measure is larger in patients with poor neurological outcome. A lighter color indicates a larger difference between the two groups.

## 4.7 INTER-VENDOR COMPARISON

In our neurological outcome population, patients scanned with the Philips Ingenia showed significantly lower whole-brain white matter FA and AFD and significantly higher MD compared to patients scanned with the Siemens Skyra (Fig. 9).

## 4.8 POST HOC ANALYSES

We performed two post hoc analyses. First, including only patients scanned with the Philips Ingenia scanner at Rijnstate (n=49; 20 with poor outcome) resulted in fewer tracts differing significantly in FA between patients with poor and good neurological outcome than in our total population (Appendix E). Tracts that remained significant in both analyses were the anterior thalamic radiation, the inferior occipito-frontal fascicle, the middle cerebral peduncle, the striatio-fronto-orbital tract, the striatio-parietal tract, the striatio-postcentral tract, the striatio-precentral tract, the striatio-prefrontal tract, the thalamo-prefrontal tract, and the thalamo-premotor tract. Tracts that did not significantly differ in FA anymore after removal of the Radboud patients, were the cingulum, inferior longitudinal fasciculus, superior cerebellar peduncle, striato-occipital tract, striato-premotor tract, thalamo-postcentral tract, and thalamo-precentral tract. We found no differences in FA, MD, and AFD between patients with normal and impaired cognition in any of the tracts (Appendix F).

Second, whole-brain white matter FA did not differ between patients with good and poor neurological outcome (Fig. 10). Whole-brain white matter AFD was significantly higher in patients with poor neurological outcome. A trend towards lower whole-brain white matter MD values in patients with poor neurological outcome compared to patients with good outcome was observed, but not statistically significant. (Fig. 10) Between patients with normal and impaired cognition were no significant differences in whole-brain white matter FA, MD, and AFD (Fig. 11).

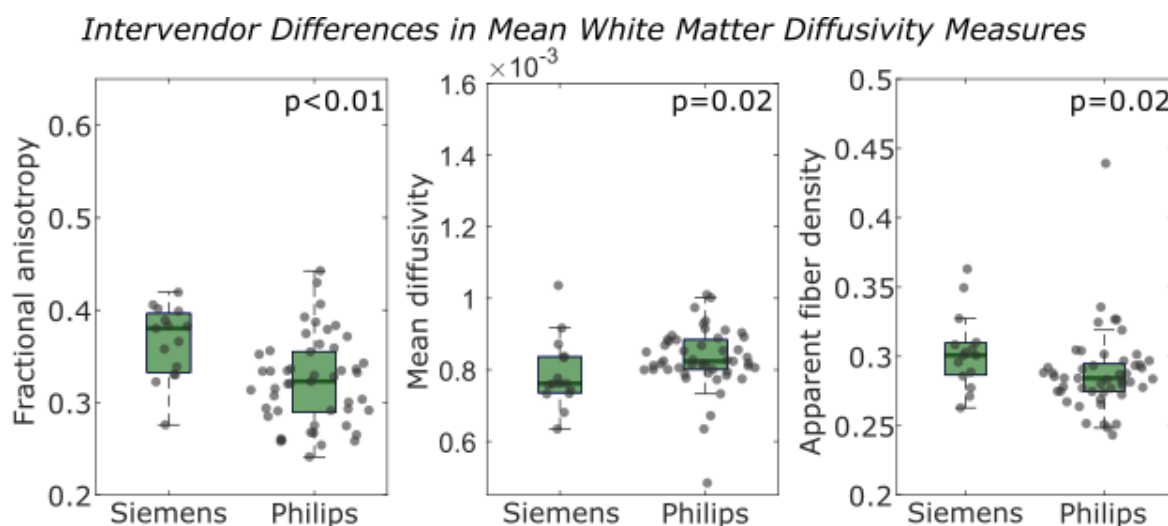


Figure 9: Mean whole-brain white matter fractional anisotropy, mean diffusivity, and apparent fiber density, grouped by scanner (Philips Ingenia or Siemens Skyra).

### Mean White Matter Diffusivity Measures and Neurological Outcome

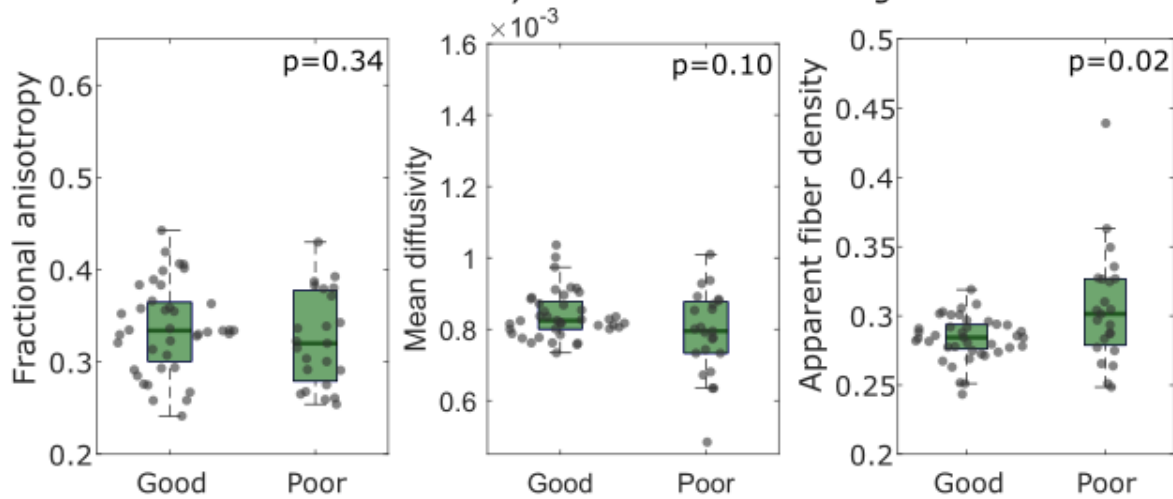


Figure 10: Mean whole-brain white matter fractional anisotropy, mean diffusivity, and apparent fiber density, grouped neurological outcome (good or poor).

### Mean White Matter Diffusivity Measures and Cognitive Performance

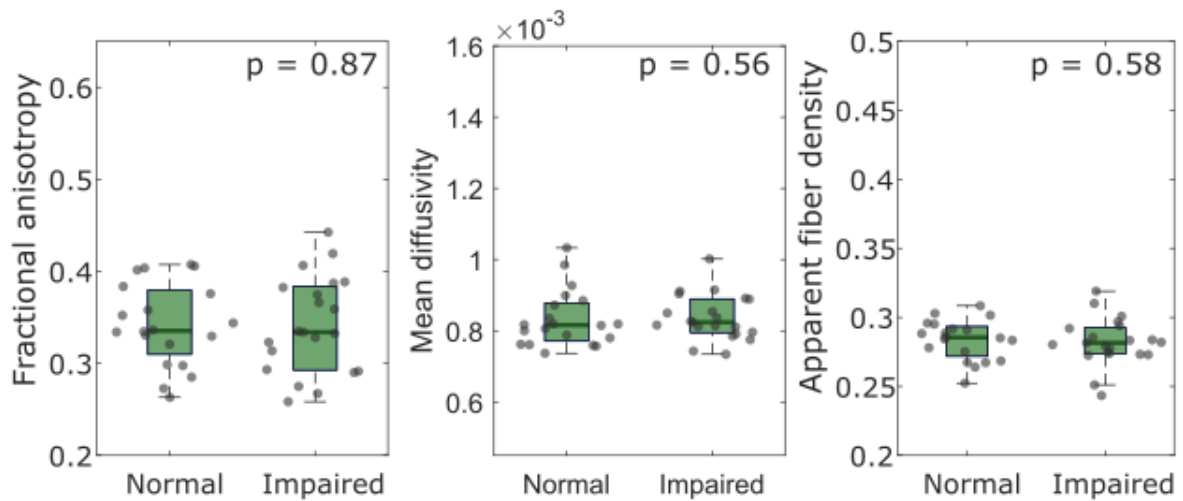


Figure 10: Mean whole-brain white matter fractional anisotropy, mean diffusivity, and apparent fiber density, grouped by cognitive performance (normal or impaired).

## 5 DISCUSSION

---

Diffusivity measures in the genu and body of the corpus callosum, the superior longitudinal fasciculus, the uncinate fasciculus, the corticospinal tract, and the thalamo-occipital tract, estimated from DTI scans obtained within the first week after cardiac arrest, were not associated with neurological outcome at six months or cognitive performance at twelve months. Exploratory analyses showed that anisotropy in the cortico-striatal tracts, thalamocortical tracts and the cerebellar peduncles was lower in patients with poor neurological outcome than in patients with good neurological outcome at six months. We found no associations between diffusivity measures in any tract and cognitive performance twelve months after cardiac arrest.

### **Diffusivity Measures and Neurological Outcome in Coma After Cardiac Arrest**

Our results differ from previous studies that analysed the anisotropy of white matter in relation to neurological outcome after cardiac arrest. Luyt *et al.* (51) looked at the mean FA of 20 white matter regions and found significantly lower FA values in patients with poor neurological outcome compared to patients with good outcome in all regions. The most pronounced differences were found in the corpus callosum and internal capsule. Patients with poor neurological outcome also had a lower whole-brain white matter FA compared to patients with good outcome according to a study by Velly *et al.* (23). These findings do not completely align with our results, as we only found differences in anisotropy between the poor and good outcome group in some of the tracts and no differences in whole-brain white matter anisotropy. This could be explained by the differences in the study population and the timing of MRI scanning. The studies mentioned above included patients who remained unresponsive for at least 7 days after cardiac arrest. These patients have a higher chance of poor neurological recovery, presumably due to more severe brain injury (52). Therefore, these studies likely included a study population with more extensive brain damage than our cohort. Furthermore, MRI scans were acquired between 7-28 days after cardiac arrest whilst most of our scans were obtained within 7 days. Since the pathophysiological processes in the brain after an anoxic event are highly dynamic (14), we probably captured different steps of the pathophysiological cascade.

Group differences in the extent of diffusion have previously been studied in relation to neurological outcome using the apparent diffusion coefficient (ADC) derived from conventional diffusion-weighted imaging (DWI). The MD is equivalent to the ADC but more robust as it is estimated from many diffusion directions instead of three. We found no difference in diffusivity in white matter within one week after cardiac arrest between patients with good neurological outcome and poor outcome, which is in line with the results of previous studies (22, 25, 26, 53). These studies did find that diffusivity was lower in patients with poor neurological outcome in cortical and deep grey matter. While we did not investigate grey matter, our subtracted MD maps showed slightly lower MD values in the cortical fiber endings in patients with poor neurological outcome. These findings suggest that the cortical white matter is also affected by oedema in the cerebral cortex. Overall, MD in grey matter is likely of greater value in outcome prediction of comatose patients after cardiac arrest than MD in white matter.

In addition to anisotropy and diffusivity, our study was the first to examine AFD in patients after cardiac arrest. Based on our hypothesis, we expected that the AFD would be higher in patients with poor neurological outcome, but this was not reflected in our results. In the average AFD maps, we did see a higher AFD located in the cortical fiber endings in patients with poor neurological outcome. Similar to

the lower MD values, these findings might imply that cytotoxic oedema is mainly present in the cortical white matter. Therefore, the AFD averaged over a complete tract is probably not an effective prognosticator for neurological outcome after cardiac arrest.

### **Diffusivity Measures and Cognitive Performance in Cardiac Arrest Survivors**

Associations between diffusivity measures and long-term cognitive performance have not been previously investigated in cardiac arrest survivors. Therefore, we here compare our population to populations with similar long-term deficits. Patients with traumatic brain injury frequently have disturbances of memory, attention and executive functioning similar to patients after cardiac arrest (54). Diffusion-tensor imaging studies in patients with traumatic brain injury showed that lower anisotropy in multiple white matter tracts, especially the corpus callosum, superior longitudinal fasciculus, uncinate fasciculus, and cingulum, were correlated with worse cognitive performance (27, 55-59). This is not in line with our current findings since we find no associations between anisotropy and cognitive performance in any white matter region. Results on magnitude of diffusivity analysed in patients with TBI were more ambiguous. Changes in MD were also correlated with measures of cognition, but directionality and height of these correlations were dependent on cognitive domain and tract and also differed per study (27, 56, 60).

Contrary to our analysis, the studies mentioned above were predominantly cross-sectional in design and performed between one to eight years after injury. The timing of their MRI scanning matched the time of cognitive testing, whereas we assessed associations between diffusivity measures obtained from MRI scans acquired within one week after resuscitation and cognitive performance months later. These differences in study design could explain some of the differences in results. Our MRI scans were mostly acquired within one week after cardiac arrest, which could be too early to detect lasting structural white matter changes. Another possibility is that changes in anisotropy and diffusivity within one week after cardiac arrest are too subtle to detect in our scan protocols. In addition, we have used a generalized screening tool to assess cognition, while the other studies used detailed neuropsychological testing in individual cognitive domains. It could be the case that disturbances in particular cognitive domains are tract-specific and that the MoCA is not sensitive enough for these disturbances.

### **Inter-Vendor Differences**

Our multicenter study combined MRI data acquired on two different types of scanners. The advantages of this multicenter design are that we can reach and include more patients and that it is an accurate representation of clinical practice. However, the use of quantitative diffusion-weighted imaging in multicenter cohorts is controversial since diffusion signals can be affected by inter-vendor differences (61). We tried to minimize this effect by harmonizing scan protocols between vendors and applying global normalization during preprocessing.

Nevertheless, we found significant inter-vendor differences in all three diffusivity measures when compared in whole-brain white matter. A post hoc analysis showed that only including patients scanned at the Rijnstate hospital resulted in fewer tracts having a statistically significant difference in anisotropy between patients with good and poor neurological outcome than in our total population. This could be explained by the fact that the Rijnstate population had a lower percentage of patients with a good neurological outcome (70%) than the Radboud population (83%). Because the anisotropy

was already higher in patients scanned at the Radboud hospital, our group differences in the total population were partially caused by vendor type instead of neurological outcome. However, some tracts in the cortico-striatal, thalamocortical and cerebellum regions remained significant. These regions therefore still hold the potential for prediction of neurological outcome in comatose patients after cardiac arrest.

Our findings are partly supported by previous studies (61, 62) on inter-vendor reliability of DTI, which only found significant differences in MD across vendors but not in FA. Anisotropy was hypothesized to be less dependent on the scanner used because the effect of vendor type on diffusivity is likely the same in all directions. The reason why we did find differences in FA across vendors could be that we used different scanners than in previous studies. Another explanation might be that more patients scanned with the Siemens scanner had a good neurological outcome. The effect of this potential bias should be further investigated.

The effects of inter-vendor differences could be minimized by alterations in our study design but would remain a challenge in clinical practice. One solution would be to only include patients from one study site, as we did in our post hoc analysis, but this would also diminish the clinical applicability of our results as scanner types vary greatly across hospitals. The second option would be to normalize our MRI data using a “travelling head” control group. For each person in the control group, diffusion-weighted scans should then be acquired on all included scanners. The diffusivity measures obtained in our study would then be normalized by scaling them by the mean measures calculated from the control group acquired with the same scanner. This method would be useful for research purposes only since this would have to be repeated for every clinical scanner and after each update of the scanner. Finally, scanner-specific cut-off values could be used, but this would be difficult to validate. For clinical implementation, a pragmatic solution towards inter-vendor differences should be investigated.

### **Strengths and Limitations**

Strengths of this study include the prospective design, the early and strict timing of the MRI scans, and the use of advanced diffusion modelling. In addition, the distribution of cognitive performance was in line with the previously reported 42-50% incidence of cognitive impairments in the general population after cardiac arrest (7).

This study also has limitations. First, our sample sizes are relatively small, especially the size of the group of patients with poor neurological outcome. The small sample size combined with the high variance in our measures could have caused a lack of power to detect possible significant group differences. Secondly, the influence of a self-fulfilling prophecy cannot be fully excluded. However, clinicians did not consider our MRI measures in the decision-making on treatment withdrawal. Finally, our acquisition design was suboptimal due to hardware and time limitations. Scans were acquired single-shell, without reverse phase encoding and with only 30-32 diffusion directions whereas 64 would be preferred. Multi-shell MRI acquisition with higher b-values and more gradients could improve the accuracy of our diffusivity measures and phase reversal would improve the registration of the scans to the standard space. Especially the AFD could be contaminated with extra-axonal signal due to our low b-values (63). While our acquisition design does lower the accuracy of representing the true underlying fiber density, it should not have a large effect on our group differences. In addition,

the acquisition of more gradients and multiple shells would be more time-consuming and thus less practical in a clinical setting.

### **Clinical Implications**

The current guidelines for post-resuscitation care recommend a multimodal approach for the prediction of poor neurological outcome in comatose patients after cardiac arrest, including clinical examination, serum biomarkers, electrophysiology, and imaging (64). The added value of tract-specific diffusivity measures to this current model should be determined starting with the most promising diffusivity measures. Based on our results, these would be the FA in the cortico-striatal tracts, thalamocortical tracts and cerebellar peduncles. If these measures show to be of added value and a solution for the inter-vendor differences is found, automated and validated pipelines could be created for clinicians to perform these analyses in a standardized fashion.

## **6 CONCLUSION**

---

Lower anisotropy in the cortico-striatal tracts, the thalamocortical tracts and the cerebellar peduncles within one week after cardiac arrest was associated with poor neurological outcome at six months. We found no associations between diffusivity measures in any white matter tract and cognitive performance at twelve months. The mean FA of individual white matter tracts holds potential for outcome prediction of comatose patients after cardiac arrest, whereas the predictive value on cognitive performance is limited. Since scanner vendor differences introduce a bias in diffusivity measures, a solution should be found before clinical application is possible.

## 7 REFERENCES

---

1. Zijlstra JA, Radstok A, Pijls R, Nas J, Beesems SG, Hulleman M, et al. Reanimatie in Nederland. 2016.
2. Hofmeijer J, Beernink TM, Bosch FH, Beishuizen A, Tjepkema-Cloostermans MC, van Putten MJ. Early EEG contributes to multimodal outcome prediction of postanoxic coma. *Neurology*. 2015;85(2):137-43.
3. Bouwes A, Binnekade JM, Kuiper MA, Bosch FH, Zandstra DF, Toornvliet AC, et al. Prognosis of coma after therapeutic hypothermia: a prospective cohort study. *Annals of Neurology*. 2012;71(2):206-12.
4. de Boer AR, van Dis I, Wimmers RH, Vaartjes I, Bots ML. Hart- en vaatziekten in Nederland. 2020.
5. Lemiale V, Dumas F, Mongardon N, Giovanetti O, Charpentier J, Chiche JD, et al. Intensive care unit mortality after cardiac arrest: the relative contribution of shock and brain injury in a large cohort. *Intensive Care Medicine*. 2013;39(11):1972-80.
6. Perez CA, Samudra N, Aiyagari V. Cognitive and Functional Consequence of Cardiac Arrest. *Current Neurology and Neuroscience Reports*. 2016;16(8):70.
7. Moulaert VR, Verbunt JA, van Heugten CM, Wade DT. Cognitive impairments in survivors of out-of-hospital cardiac arrest: a systematic review. *Resuscitation*. 2009;80(3):297-305.
8. Goossens PH, Moulaert VR. Cognitive impairments after cardiac arrest: implications for clinical daily practice. *Resuscitation*. 2014;85(12):A3-4.
9. Sauve MJ, Doolittle N, Walker JA, Paul SM, Scheinman MM. Factors associated with cognitive recovery after cardiopulmonary resuscitation. *American Journal of Critical Care*. 1996;5(2):127-39.
10. Groswasser Ze, Cohen M, Costeff H. Rehabilitation Outcome After Anoxic Brain Damage. *Archives of Physical Medicine and Rehabilitation*. 1989;70(3):186-8.
11. Alem AP, van., Vos R, de., Schmand B, Koster RW. Cognitive impairment in survivors of out-of-hospital cardiac arrest. *American Heart Journal*. 2004;148(3):416-21.
12. Medrzycka-Dabrowska WA, Czyz-Szybenbejl K, Kwiecien-Jagus K, Lewandowska K. Prediction of cognitive dysfunction after resuscitation - a systematic review. *Postepy Kardiologii Interwencyjnej*. 2018;14(3):225-32.
13. van den Brule JMD, van der Hoeven JG, Hoedemaekers CWE. Cerebral Perfusion and Cerebral Autoregulation after Cardiac Arrest. *Biomed Res Int*. 2018;2018:4143636.
14. Sandroni C, Cronberg T, Sekhon M. Brain injury after cardiac arrest: pathophysiology, treatment, and prognosis. *Intensive Care Med*. 2021;47(12):1393-414.
15. Greer D, Scripko P, Bartscher J, Sims J, Camargo E, Singhal A, et al. Serial MRI Changes in Comatose Cardiac Arrest Patients. *Neurocritical Care*. 2010;14(1):61-7.
16. Liang D, Bhatta S, Gerzanich V, Simard JM. Cytotoxic edema: mechanisms of pathological cell swelling. *Neurosurgical Focus*. 2007;22(5):E2.
17. Basser PJ, Jones DK. Diffusion-tensor MRI: theory, experimental design and data analysis - a technical review. *NMR in Biomedicine*. 2002;15(7-8):456-67.
18. Conturo TE, Lori NF, Cull TS, Akbudak E, Snyder AZ, Shimony JS, et al. Tracking neuronal fiber pathways in the living human brain. *Proc Natl Acad Sci U S A*. 1999;96(18):10422-7.
19. Huisman TA. Diffusion-weighted and diffusion tensor imaging of the brain, made easy. *Cancer Imaging*. 2010;10 Spec no A:S163-71.
20. Soares JM, Marques P, Alves V, Sousa N. A hitchhiker's guide to diffusion tensor imaging. *Frontiers in Neuroscience*. 2013;7:31.
21. Raffelt D, Tournier JD, Rose S, Ridgway GR, Henderson R, Crozier S, et al. Apparent Fibre Density: a novel measure for the analysis of diffusion-weighted magnetic resonance images. *Neuroimage*. 2012;59(4):3976-94.

22. Keijzer HM, Duering M, Pasternak O, Meijer FJA, Verhulst M, Tonino BAR, et al. Free water corrected diffusion tensor imaging discriminates between good and poor outcomes of comatose patients after cardiac arrest. *European Radiology*. 2022.
23. Velly L, Perlberg V, Boulier T, Adam N, Delphine S, Luyt C-E, et al. Use of brain diffusion tensor imaging for the prediction of long-term neurological outcomes in patients after cardiac arrest: a multicentre, international, prospective, observational, cohort study. *The Lancet Neurology*. 2018;17(4):317-26.
24. van der Eerden AW, Khalilzadeh O, Perlberg V, Dinkel J, Sanchez P, Vos PE, et al. White matter changes in comatose survivors of anoxic ischemic encephalopathy and traumatic brain injury: comparative diffusion-tensor imaging study. *Radiology*. 2014;270(2):506-16.
25. Youn CS, Park KN, Kim JY, Callaway CW, Choi SP, Rittenberger JC, et al. Repeated diffusion weighted imaging in comatose cardiac arrest patients with therapeutic hypothermia. *Resuscitation*. 2015;96:1-8.
26. Wu O, Sorensen AG, Benner T, Singhal AB, Furie KL, Greer DM. Comatose patients with cardiac arrest: predicting clinical outcome with diffusion-weighted MR imaging. *Radiology*. 2009;252(1):173-81.
27. Gu L, Li J, Feng DF, Cheng ET, Li DC, Yang XQ, et al. Detection of white matter lesions in the acute stage of diffuse axonal injury predicts long-term cognitive impairments: a clinical diffusion tensor imaging study. *Journal of Acute care and Surgery*. 2013;74(1):242-7.
28. Matsushita M, Hosoda K, Naitoh Y, Yamashita H, Kohmura E. Utility of diffusion tensor imaging in the acute stage of mild to moderate traumatic brain injury for detecting white matter lesions and predicting long-term cognitive function in adults. *Journal of Neurosurgery*. 2011;115(1):130-9.
29. van Gils P, van Heugten C, Hofmeijer J, Keijzer H, Nutma S, Duits A. The Montreal Cognitive Assessment is a valid cognitive screening tool for cardiac arrest survivors. *Resuscitation*. 2021.
30. Veraart J, Novikov DS, Christiaens D, Ades-Aron B, Sijbers J, Fieremans E. Denoising of diffusion MRI using random matrix theory. *Neuroimage*. 2016;142:394-406.
31. Kellner E, Dhital B, Kiselev VG, Reiser M. Gibbs-ringing artifact removal based on local subvoxel-shifts. *Magnetic Resonance in Medicine*. 2016;76(5):1574-81.
32. Smith SM. Fast robust automated brain extraction. *Human Brain Mapping*. 2002;17(3):143-55.
33. Fischl B. FreeSurfer. *Neuroimage*. 2012;62(2):774-81.
34. Schilling KG, Blaber J, Hansen C, Cai L, Rogers B, Anderson AW, et al. Distortion correction of diffusion weighted MRI without reverse phase-encoding scans or field-maps. *PLoS One*. 2020;15(7):e0236418.
35. Andersson JLR, Skare S, Ashburner J. How to correct susceptibility distortions in spin-echo echo-planar images: application to diffusion tensor imaging. *NeuroImage*. 2003;20(2):870-88.
36. Smith SM, Jenkinson M, Woolrich MW, Beckmann CF, Behrens TE, Johansen-Berg H, et al. Advances in functional and structural MR image analysis and implementation as FSL. *Neuroimage*. 2004;23 Suppl 1:S208-19.
37. Andersson JLR, Sotiropoulos SN. An integrated approach to correction for off-resonance effects and subject movement in diffusion MR imaging. *Neuroimage*. 2016;125:1063-78.
38. Avants B, Tustison NJ, Song G. Advanced Normalization Tools: V1.0. *The Insight Journal*. 2009.
39. Wasserthal J, Neher P, Maier-Hein KH. TractSeg - Fast and accurate white matter tract segmentation. *Neuroimage*. 2018;183:239-53.
40. Tournier JD, Mori S, Leemans A. Diffusion tensor imaging and beyond. *Magnetic Resonance in Medicine*. 2011;65(6):1532-56.
41. Siegbahn M, Engmer Berglin C, Moreno R. Automatic segmentation of the core of the acoustic radiation in humans. *Frontiers in Neurology*. 2022;13:934650.
42. O'Donnell LJ, Westin CF. An introduction to diffusion tensor image analysis. *Neurosurgery Clinics of North America*. 2011;22(2):185-96, viii.

43. Garyfallidis E, Brett M, Amirbekian B, Rokem A, van der Walt S, Descoteaux M, et al. Dipy, a library for the analysis of diffusion MRI data. *Frontiers in Neuroinformatics*. 2014;8:8.
44. Tournier JD, Calamante F, Gadian DG, Connelly A. Direct estimation of the fiber orientation density function from diffusion-weighted MRI data using spherical deconvolution. *Neuroimage*. 2004;23(3):1176-85.
45. Dell'Acqua F, Tournier JD. Modelling white matter with spherical deconvolution: How and why? *NMR Biomed*. 2019;32(4):e3945.
46. Tournier J-DS, R.E. Raffelt, D. Tabbara, R. Dhollander, T. Pietsch, M. Christiaens, D. Jeurissen, B. Yeh, C.-H. Connelly, A. . MRtrix3: A fast, flexible and open software framework for medical image processing and visualisation. *Neuroimage*. 2019(202):116-37.
47. Jenkinson M. Improved Optimization for the Robust and Accurate Linear Registration and Motion Correction of Brain Images. *NeuroImage*. 2002;17(2):825-41.
48. Jenkinson M, Smith S. A global optimisation method for robust affine registration of brain images. *Medical Image Analysis*. 2001;5(2):143-56.
49. Zhang Y, Brady M, Smith S. Segmentation of brain MR images through a hidden Markov random field model and the expectation-maximization algorithm. *IEEE Trans Medicine Imaging*. 2001;20(1):45-57.
50. Benjamini Y, Yekutieli D. The control of the false discovery rate in multiple testing under dependency. *The Annals of Statistics*. 2001;29(4).
51. Luyt CE, Galanaud D, Perlberg V, Vanhauzenhuysse A, Stevens RD, Gupta R, et al. Diffusion tensor imaging to predict long-term outcome after cardiac arrest: a bicentric pilot study. *Anesthesiology*. 2012;117(6):1311-21.
52. Levy DE. Predicting Outcome From Hypoxic-Ischemic Coma. *JAMA: The Journal of the American Medical Association*. 1985;253(10).
53. Mlynash M, Campbell DM, Leproust EM, Fischbein NJ, Bammer R, Eyngorn I, et al. Temporal and spatial profile of brain diffusion-weighted MRI after cardiac arrest. *Stroke*. 2010;41(8):1665-72.
54. Arciniegas DB, Held K, Wagner P. Cognitive Impairment Following Traumatic Brain Injury. *Current Treatment Options in Neurology*. 2002;4(1):43-57.
55. Kraus MF, Susmaras T, Caughlin BP, Walker CJ, Sweeney JA, Little DM. White matter integrity and cognition in chronic traumatic brain injury: a diffusion tensor imaging study. *Brain*. 2007;130(Pt 10):2508-19.
56. Arenth PM, Russell KC, Scanlon JM, Kessler LJ, Ricker JH. Corpus callosum integrity and neuropsychological performance after traumatic brain injury: a diffusion tensor imaging study. *The Journal of Head Trauma Rehabilitation*. 2014;29(2):E1-E10.
57. Geary EK, Kraus MF, Pliskin NH, Little DM. Verbal learning differences in chronic mild traumatic brain injury. *Journal of the International Neuropsychological Society*. 2010;16(3):506-16.
58. Palacios EM, Sala-Llonch R, Junque C, Fernandez-Espejo D, Roig T, Tormos JM, et al. Long-term declarative memory deficits in diffuse TBI: correlations with cortical thickness, white matter integrity and hippocampal volume. *Cortex*. 2013;49(3):646-57.
59. Spitz G, Maller JJ, O'Sullivan R, Ponsford JL. White matter integrity following traumatic brain injury: the association with severity of injury and cognitive functioning. *Brain Topogr*. 2013;26(4):648-60.
60. Grossman EJ, Jensen JH, Babb JS, Chen Q, Tabesh A, Fieremans E, et al. Cognitive impairment in mild traumatic brain injury: a longitudinal diffusional kurtosis and perfusion imaging study. *AJNR Am J Neuroradiol*. 2013;34(5):951-7, S1-3.
61. Min J, Park M, Choi JW, Jahng GH, Moon WJ. Inter-Vendor and Inter-Session Reliability of Diffusion Tensor Imaging: Implications for Multicenter Clinical Imaging Studies. *Korean J Radiol*. 2018;19(4):777-82.
62. Pagani E, Hirsch JG, Pouwels PJ, Horsfield MA, Perego E, Gass A, et al. Intercenter differences in diffusion tensor MRI acquisition. *J Magn Reson Imaging*. 2010;31(6):1458-68.
63. Genc S, Tax CMW, Raven EP, Chamberland M, Parker GD, Jones DK. Impact of b-value on estimates of apparent fibre density. *Human Brain Mapping*. 2020;41(10):2583-95.

64. Nolan JP, Sandroni C, Bottiger BW, Cariou A, Cronberg T, Friberg H, et al. European Resuscitation Council and European Society of Intensive Care Medicine guidelines 2021: post-resuscitation care. *Intensive Care Med.* 2021;47(4):369-421.
65. Tax CMW, Vos SB, Leemans A. Checking and Correcting DTI Data. *Diffusion Tensor Imaging.* 1 ed. New York: Springer; 2016. p. 127-50.
66. Brooks JC, Faull OK, Pattinson KT, Jenkinson M. Physiological noise in brainstem FMRI. *Front Hum Neurosci.* 2013;7:623.
67. Archibald R, Gelb A. A method to reduce the Gibbs ringing artifact in MRI scans while keeping tissue boundary integrity. *IEEE Trans Med Imaging.* 2002;21(4):305-19.
68. Yang XQ, Smith MB, Wang J. Magnetic Susceptibility Effects in High Field MR. *Ultra High Field Magnetic Resonance Imaging.* 1 ed. New York: Springer; 2006. p. 249-84.
69. Schilling KG, Blaber J, Huo Y, Newton A, Hansen C, Nath V, et al. Synthesized b0 for diffusion distortion correction (Synb0-DisCo). *Magn Reson Imaging.* 2019;64:62-70.
70. Zhuang J, Hrabe J, Kangarlu A, Xu D, Bansal R, Branch CA, et al. Correction of eddy-current distortions in diffusion tensor images using the known directions and strengths of diffusion gradients. *J Magn Reson Imaging.* 2006;24(5):1188-93.
71. Le Bihan D, Poupon C, Amadon A, Lethimonnier F. Artifacts and pitfalls in diffusion MRI. *J Magn Reson Imaging.* 2006;24(3):478-88.
72. Sled JG, Zijdenbos AP, Evans AC. A nonparametric method for automatic correction of intensity nonuniformity in MRI data. *IEEE Trans Med Imaging.* 1998;17(1):87-97.
73. Larsen CT, Iglesias JE, Van Leemput K. N3 Bias Field Correction Explained as a Bayesian Modeling Method. *Bayesian and graphical Models for Biomedical Imaging: Springer, Cham;* 2014. p. 1-12.
74. Kinnunen KM, Greenwood R, Powell JH, Leech R, Hawkins PC, Bonnelle V, et al. White matter damage and cognitive impairment after traumatic brain injury. *Brain.* 2011;134(Pt 2):449-63.
75. Chiou KS, Jiang T, Chiaravalloti N, Hoptman MJ, DeLuca J, Genova H. Longitudinal examination of the relationship between changes in white matter organization and cognitive outcome in chronic TBI. *Brain Inj.* 2019;33(7):846-53.

## Appendix A. OVERVIEW PREPROCESSING AND PROCESSING SCRIPTS

Table 4: Scripts for preprocessing and processing of the diffusion data are written in Bash. The first few scripts run for individual patients. Later in the pipeline, the scripts run for individual tracts. All scripts have a supplementary script with the suffix ‘\_run’ to loop the script over multiple patients or tracts at once. Scripts that run for the complete set of patients have the suffix “\_group”. The scripts should always run in the specific order shown in the table with the same folder structure.

Name script	Function	To change manually	Input and output	Time est.
<i>Preprocessing</i>				
DTI_preproc_Nienke_part1.sh	Applies the following preprocessing steps: denoising, degibbs, b0 extraction and brain masking, T1 normalization, T1 skull stripping, registration of b0 to T1 and linear and non-linear transformation of b0 and T1 to MNI atlas 152.	<b>niifolder:</b> bidsfolder <b>destfolder:</b> output directory for preprocessing files.	<b>In:</b> - Bids folder for each patient containing a DTI and T1 scan. <b>Out:</b> - Denoised and degibbs DTI scan. - Preprocessed T1 image. - T1 and b0 image in atlas space. - Registration matrix to atlas space.	± 1h
DTI_preproc_Nienke_part2.sh	Runs inference.py to generate 5 undistorted b0 images. Needs to be submitted to the GPU. For speed, the preprocessing pipeline is divided into three parts and only this part is submitted to the GPU.	<b>destfolder:</b> output directory for preprocessing files. <b>DISCOfolder:</b> directory towards the synb0-DISCO folder.	<b>In:</b> - T1 and b0 image in atlas space. <b>Out:</b> - 5 estimates of an undistorted b0 image.	± 2min
DTI_preproc_Nienke_part3.sh	Takes the average of the 5 estimated undistorted b0 images and transforms this image back to subject space. Runs TOPUP with the generated b0 image. Next the final preprocessing scripts are applied: Eddy, bias field correction, and global normalization.	<b>destfolder:</b> output directory for preprocessing files. <b>DISCOfolder:</b> directory towards the synb0-DISCO folder.	<b>In:</b> - 5 estimates of an undistorted b0 image. - Registration matrix to atlas space. - Denoised and degibbs DTI image. <b>Out:</b> - Preprocessed DTI image. - Final brain mask.	± 3h
Copy_preproc_files.sh	Copies the data from preprocessing to new folders for processing. First, manually create the folder you want to copy the data to (for example <i>metrics</i> or <i>tractography</i> ).	<b>destfolder:</b> empty folder you want the data to copy to. <b>preprocfolder_RIJN/RAD:</b> folder containing the preprocessed grouped in folders per subject from either Rijnstate or Radboud patients.	<b>In/out:</b> - Preprocessed DTI image. - T1 image. - Final brain mask - bvals generated by eddy. - bvecs.	<1min
Copy_preproc_files_BROCA.sh	Repeats the same copying steps for the BROCA-data.	<b>destfolder:</b> empty folder you want the data to copy to. <b>preprocfolder_RIJN:</b> folder containing the preprocessed grouped in folders per subject.	<b>In/out:</b> - Preprocessed DTI image. - T1 image. - Final brain mask - bvals generated by eddy. - bvecs.	<1min
<i>Compute FA and MD</i>				
Metrics.sh	Calculates the FA, the MD, and the RD and AD (not used in our analysis).	<b>inputfolder:</b> folder containing folder for each patient with the copied data from the preprocessing pipeline.	<b>In:</b> - Preprocessed DTI image. - bvals from eddy and bvecs. - Final brain mask. <b>Out:</b> - FA and MD maps.	<1min
<i>Compute the AFD</i>				
Individual_response.sh	Computes the individual response function for each subject.	<b>folder:</b> should be the path to the same folder as the destfolder in the metrics script.	<b>In:</b> - Preprocessed DTI image. - bvals from eddy and bvecs. - Final brain mask. <b>Out:</b>	<1min

			- Individual response function for white matter, grey matter and CSF.	
Average_response_group.sh	Calculates the average response function for white matter and CSF of all the subjects.	<b>destfolder:</b> the same folder as the destfolder in metrics.sh	<b>In:</b> - individual response functions of all subjects. <b>Out:</b> - The average response function for white matter and CSF.	<1min
ApparentFiberDensity.sh	Calculated the fiber Orientation Distribution Function for each subject with two shells.	<b>destfolder:</b> the same folder as the destfolder in metrics.sh	<b>In:</b> - Preprocessed DTI image. - The average response function for white matter and CSF. <b>Out:</b> - fODF for each patient.	± 10min
<b>TractSeg</b>				
TractSeg.sh	Runs the following TractSeg steps: peak extraction, endings segmentation, tract orientation mapping, and tracking.	<b>destfolder:</b> folder used for the output of tractseg containing the copied preprocessed data.	<b>In:</b> - Preprocessed DTI image. - bvals from eddy and bvecs. <b>Out:</b> - endings and tract segmentations. - .tck files of 72 tracts.	± 45min
<b>Combining tracts and metrics</b>				
Metrics2MNI.sh	Transforms the FA, MD, and AFD maps to MNI space using the transformation matrix obtained from TractSeg.	<b>Transformfolder:</b> folder containing the output data from tractseg. <b>inputfolder:</b> folder containing the FA, MD, and AFD maps.	<b>In:</b> - FA2MNI.mat file. - FA, MD, and AFD maps. <b>Out:</b> - FA, MD, and AFD maps in MNI space.	<1min
BundleMetrics.sh	Samples the metrics over the streamline and takes the mean each streamline. The mean FA, MD, and AFD per streamline are saved in a test file. The folder-structure in which the .txt files are saved is now changed with respect to the previous structure. The text files are saved per tract instead of per subject. This means that each tract has a separate folder containing the .txt files for each subject.	<b>metricsfolder:</b> folder containing the FA, MD, and AFD maps. <b>tractseffolder:</b> folder containing the tractseg output. <b>outputfolder:</b> output folder for bundle metrics.	<b>In:</b> - FA, MD, and AFD maps in MNI space. - TractSeg .tck files. <b>Out:</b> - text files of the mean FA, MD, and AFD per streamline.	± 5 min

## Appendix B. BACKGROUND: PREPROCESSING OF DIFFUSION MRI

Like any other MRI technique, diffusion MRI is subject to artifacts (65). The presence of artifacts can adversely affect the accuracy and precision of diffusion measures. Therefore, preprocessing is essential to obtain reliable results during processing. (20) In the following subchapters, the most common artifacts in diffusion MRI and our preprocessing steps to overcome them are explained.

### A1. Noise

In MRI, random background noise primarily originates from thermal fluctuations within the subject and within the receiver electronics (66). To remove noise from an image, the difference between signal and noise needs to be distinguished. We used the denoising method as implemented in *mrdenoise* in MRtrix3, which makes use of the Marchenko-Pastur Principal Component Analysis (MP-PCA) algorithm (30). This algorithm transforms the dataset into a principal component basis. Afterwards, only the signal-carrying principal components are preserved, whereas noise is removed using thresholding the eigenvalues of the components.

### A2. Gibbs ringing

The Gibbs ringing artifact occurs close to tissue boundaries with strong intensity differences. The artifact results from the Fourier technique that is used to reconstruct the images. MR images are approximated with a limited number of frequencies on a discrete grid. (67) How the grid is sampled, can influence the strength of the Gibbs-ringing artefact. When the sinc function is sampled at its minimum and maximum peak at an abrupt tissue transition, the ringing amplitude becomes maximal (Fig. 12a). When the sinc function is sampled at the zero-crossing, the ringing amplitude disappears (Fig. 12b). Gibbs-ringing artefacts can therefore be removed by resampling the image such that the sinc function has its zero-crossings around strong tissue boundaries (31). We performed this resampling using *mrdegibbs* in MRtrix3.

### A3. Susceptibility induced distortions

Magnetic susceptibility describes how a material is magnetized when exposed to a magnetic field. When the difference in susceptibility between two neighbouring tissues is large, this results in the induction of an additional magnetic field that distorts the  $B_0$  field. In the brain, this effect is mostly present in areas close to the air-filled sinuses such as in the frontal and temporal lobes. (68) This results in signal accumulation, where the signal of multiple voxels is piled up into one voxel, or signal “smearing”, where the signal from one voxel is stretched over multiple voxels (65). It depends on the direction of the phase-encoding which of these two effects occurs.

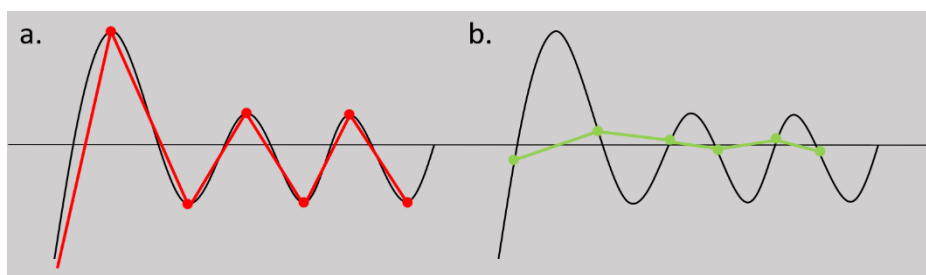


Figure 12: Sampling of a sinc-function on a discrete grid, where (a) leads to a Gibbs ringing artefact, because the sinc function is sampled at the minimum and maximum peak and (b) leads to a minimal Gibbs ringing effect, because de sinc function is sampled at the zero-crossing.

A widely applied strategy for susceptibility distortion correction is to use a pair of b0-images with reverse phase encoding gradients and warp them to the midway point between them to derive an undistorted image. This technique is available in FSL under the name TOPUP. (36) However, our imaging protocol did not include the acquisition of two images with opposing phase encoding directions. To enable TOPUP with a single distorted diffusion image, we used the Synb0-DISCO technique (34, 69). Synb0-DISCO creates an undistorted b0 image by registration of the distorted b0 image to a structural T1 image. The synthesized, undistorted image together with the distorted image could then be used as input for TOPUP.

The input for the Synb0-DISCO pipeline was the distorted b0 image and the structural T1 image. The pipeline started by preparing the T1 image with bias field correction, intensity normalization, and skull stripping in FreeSurfer (33). Subsequently, the distorted b0 image was registered to the T1 image with a rigid body with six degrees of freedom transformation (36) in FSL. Both the T1 and b0 images were transformed to MNI space. The average of five neural networks, that were trained using 5-fold cross-validation on 850 subjects, was taken to get a synthesized undistorted b0 image in MNI space. The undistorted b0 image was then warped back from MNI space to subject space using the inverse transform. This final undistorted b0 image was merged with the distorted b0 image and passed into TOPUP (35) together with an acquisition parameters file. This file contained one row for each image consisting of four columns that specify the phase encoding axis and the read-out-time. For the undistorted image, the read-out-time was zero, which let TOPUP know that the second volume contains no susceptibility distortion. The application of TOPUP resulted in a diffusion image corrected for susceptibility distortion, which can be used as input into FSL's Eddy.

#### **A4. Eddy current-induced distortions and motion artefacts**

Diffusion MRI is often performed with Echo-Planar Imaging (EPI), which uses rapidly switching gradient pulses. The constant switching gradient causes conductors in the magnetic field to generate electrical currents. These so-called Eddy currents lead to a wide range of image artifacts including geometric distortions, blurring, and shading. (70)

Motion artefacts are also the result of the strong gradient pulses used in EPI and can arise between diffusion volumes as well as in individual slices. A standard diffusion MRI sequence takes around five to ten minutes, and it is difficult to avoid all subject movement during this timeframe. This is especially the case for our subjects that are non-comatose during MRI since they often experience chest pain or might be delirious during the acquisition making it more difficult to lay completely still. The motion of brain tissue can also be caused by the inflow of blood. All movements cause a displacement of water molecules that is much larger than the displacement caused by diffusion. Since EPI collects even and odd-numbered slices sequentially, this leads to interslice instabilities.

The Eddy tool in FSL (37) was used to correct for both eddy current-induced distortions as well as motion artifacts. This tool uses an estimate of the eddy-current induced field and subject position to unwarped the diffusion volumes. From the unwarped image, the diffusion image is modelled using a Gaussian Process. This model is a prediction of how each diffusion image should look like. This prediction is compared to the observed reality and then used to update the estimation of the eddy current-induced field and the subject position. These new estimations are then again used to unwarped the diffusion volumes. This process is repeated for a set number of iterations. (65, 71)

#### A5. Bias field inhomogeneities

Bias field correction was performed with the Non-parametric Non-uniform Normalization (N3) technique as implemented in Freesurfer (72). The N3 technique assumes that the MRI signal is blurred due to a convolution of the underlying image and the bias field, where the bias field is assumed to have the shape of zero-mean Gaussian with known variance. The N3 algorithm then performs deconvolution to estimate a smooth bias field model with an iterative process. The uncorrected data is then divided by the bias field estimate to obtain an image without bias field inhomogeneities. (73)

#### A6. Global intensity normalization

Global intensity normalization is essential when comparing subjects based on parameters that are dependent on intensity levels. We normalized the intensity using *mri\_normalize* as implemented in MRtrix3. This method normalizes the images based on the median intensity value within a supplied white matter mask. This mask was created by calculating and thresholding the fractional anisotropy in each voxel. The median intensity value within this mask is different for each subject, but for every subject, this median was divided by the same specified value (default=1000). By multiplying the complete volume with this ratio, the intensity was normalized across subjects. (46)

## Appendix C. SELECTION OF TRACTS FOR THE PRIMARY ANALYSIS

Table 5: List of tracts that showed significant associations or correlations with neurological outcome or cognitive performance in previous studies in patients after cardiac arrest or traumatic brain injury (TBI). The study designs in which the tracts were studied are green, with the following categories: (1) a study on an FA-based model to predict neurological outcome in patients after cardiac arrest (the model of the three green tracts combined had the highest sensitivity and specificity) (51), (2) a study that showed significant differences in FA between patients after cardiac arrest and healthy controls (24), (3) a prognostic study in TBI patients that showed a correlation between early FA measurements and long-term cognitive impairments (27), and (4) studies that show a cross-sectional correlation between diffusivity measure and cognitive impairments in TBI patients (55-59, 74, 75). The order of the categories is the order of importance to our decision of tract selection.

Population	Patients after Cardiac Arrest		Patients with TBI	
Type of research	Prediction Model	Patients vs. Controls	Prognostic	Cross-Sectional
<b>Genu CC</b>				
<b>Body CC</b>				
Splenium CC				
<b>Superior longitudinal fasciculus</b>				
<b>Posterior limb of internal capsule</b>				
Corona radiata				
<b>Sagittal Stratum</b>				
External capsule				
Cingulum				
Uncinate fasciculus				
Inferior longitudinal fasciculus				
Anterior brainstem				
Posterior brainstem				
Cerebral peduncles				

### D1. SELECTION OF TRACTS FROM WHITE MATTER REGIONS

We selected the following white matter regions based on Table 6: the genu and body of the corpus callosum, the superior longitudinal fasciculus, the posterior limb of the internal capsule, and the sagittal stratum. Then, we chose five tracts that passed through these regions for our primary analysis (Fig. 13).

#### D1.1 Body and genu of the corpus callosum

We combined the body and genu of the corpus callosum as one tract in our primary analysis. We chose to combine the tracts, because in a previous study, both tracts were included in an FA-based model that could predict neurological outcome after cardiac arrest with the highest sensitivity and specificity compared to models with other white matter regions (51). In addition, diffusivity measures in both tracts were found to correlate with cognitive performance in patients after traumatic brain injury (55-57, 59, 74). Changes in the body and genu of the corpus callosum therefore seem to affect both neurological outcome and cognitive performance.

#### D1.2 Superior longitudinal fasciculus

Part I, II, and III of the superior longitudinal fasciculus were segmented as individual tracts in TractSeg, but we combined them into one tract for our analysis. This was also common practice in previous studies (24, 27).

### D1.3 Corticospinal tract

The corticospinal tract was included in our primary analysis because it passes through both the sagittal stratum and the posterior limb of the internal capsule.

### D1.4 Thalamo-occipital tract

The thalamo-occipital tract does not pass through one of the selected white matter regions, but was included in our analysis because of a previous study in our cohort (22). In this study, a voxel-based comparison was performed between patients with good and poor neurological outcome after cardiac arrest. The results showed that the fractional anisotropy was lower in patients with poor neurological outcome throughout the whole white matter, but especially in the occipital regions. We included the thalamo-occipital tract as it is mostly located in the occipital region of the brain.

### D1.5 Uncinate fasciculus

Because we already included tracts from each selected white matter region, we also decided to add the uncinate fasciculus to include a frontal tract. Our primary analysis therefore included tracts of different sizes throughout the whole brain.

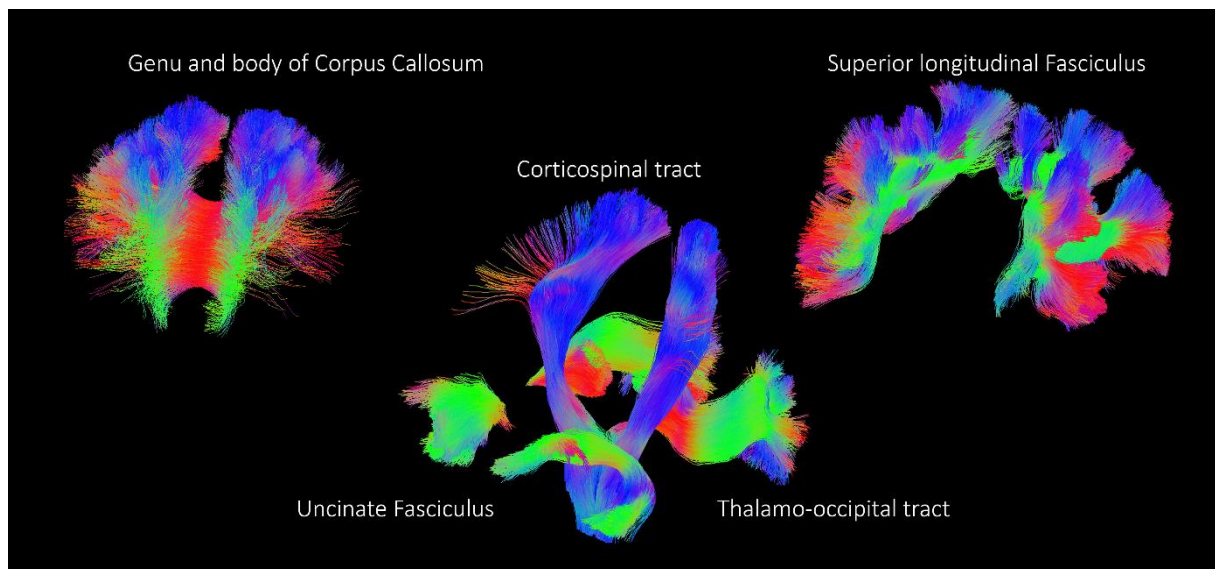


Figure 13: Final selection of the tracts included in our primary analysis.

## Appendix D. MEDIAN DIFFUSIVITY MEASURES PER TRACT GROUPED BY COGNITIVE PERFORMANCE

Table 6: Median [IQR] fractional anisotropy (FA), mean diffusivity (MD), and apparent fiber density (AFD) in 28 white matter tracts throughout the whole brain, grouped by cognitive performance (normal or impaired).

Metric	FA		MD (*10 <sup>-3</sup> )		AFD	
	Normal (n=20)	Impaired (n=20)	Normal (n=20)	Impaired (n=20)	Normal (n=20)	Impaired (n=20)
Cognitive performance						
Arcuate fascicle	0.40 [0.38-0.41]	0.38 [0.36-0.40]	0.76 [0.73-0.78]	0.78 [0.76-0.81]	0.29 [0.28-0.30]	0.28 [0.27-0.29]
Anterior thalamic radiation	0.37 [0.34-0.38]	0.34 [0.32-0.38]	0.84 [0.81-0.89]	0.87 [0.85-0.89]	0.27 [0.25-0.28]	0.25 [0.25-0.26]
Commissure anterior	0.31 [0.27-0.37]	0.30 [0.25-0.37]	0.87 [0.83-0.97]	0.91 [0.82-0.95]	0.22 [0.20-0.24]	0.21 [0.17-0.23]
Rostrum (Corpus Callosum)	0.44 [0.41-0.48]	0.42 [0.38-0.45]	0.89 [0.84-0.94]	0.90 [0.88-0.96]	0.25 [0.23-0.27]	0.23 [0.23-0.24]
Isthmus (Corpus Callosum)	0.47 [0.44-0.50]	0.46 [0.43-0.49]	0.92 [0.89-0.97]	0.75 [0.90-1.00]	0.27 [0.26-0.28]	0.27 [0.26-0.28]
Splenium (Corpus Callosum)	0.51 [0.48-0.53]	0.49 [0.46-0.51]	1.00 [0.96-1.10]	1.00 [0.99-1.10]	0.27 [0.26-0.28]	0.27 [0.26-0.29]
Cingulum	0.40 [0.38-0.42]	0.38 [0.36-0.41]	0.77 [0.75-0.81]	0.80 [0.77-0.82]	0.29 [0.27-0.29]	0.28 [0.27-0.29]
Fronto-pontine tract	0.48 [0.46-0.51]	0.46 [0.43-0.48]	0.79 [0.74-0.81]	0.79 [0.76-0.82]	0.29 [0.27-0.31]	0.28 [0.27-0.30]
Inferior occipito-frontal fascicle	0.42 [0.40-0.44]	0.40 [0.39-0.42]	0.87 [0.83-0.93]	0.89 [0.86-0.93]	0.28 [0.26-0.28]	0.27 [0.26-0.28]
Inferior longitudinal fasciculus	0.42 [0.40-0.45]	0.41 [0.39-0.42]	0.84 [0.81-0.88]	0.87 [0.85-0.90]	0.26 [0.26-0.28]	0.27 [0.26-0.28]
Middle cerebellar peduncle	0.49 [0.47-0.50]	0.47 [0.46-0.50]	0.79 [0.74-0.81]	0.77 [0.74-0.83]	0.31 [0.29-0.32]	0.31 [0.29-0.34]
Middle longitudinal fasciculus	0.38 [0.36-0.41]	0.37 [0.35-0.40]	0.82 [0.79-0.85]	0.85 [0.81-0.86]	0.28 [0.27-0.29]	0.27 [0.27-0.28]
Optic radiation	0.43 [0.41-0.46]	0.42 [0.41-0.44]	0.88 [0.85-0.94]	0.89 [0.86-0.94]	0.27 [0.26-0.27]	0.27 [0.26-0.28]
Parieto-occipital pontine	0.48 [0.46-0.49]	0.46 [0.44-0.49]	0.84 [0.80-0.87]	0.85 [0.81-0.86]	0.29 [0.28-0.30]	0.29 [0.28-0.30]
Superior cerebellar peduncle	0.45 [0.44-0.47]	0.42 [0.41-0.47]	0.86 [0.84-0.91]	0.87 [0.85-0.95]	0.29 [0.28-0.31]	0.30 [0.28-0.31]
Striato-fronto-orbital tract	0.35 [0.33-0.38]	0.33 [0.30-0.36]	0.84 [0.80-0.89]	0.86 [0.84-0.88]	0.26 [0.24-0.28]	0.24 [0.24-0.26]
Striato-occipital tract	0.44 [0.42-0.46]	0.43 [0.41-0.45]	0.87 [0.84-0.91]	0.89 [0.86-0.95]	0.28 [0.27-0.28]	0.27 [0.27-0.28]
Striato-parietal tract	0.41 [0.39-0.42]	0.39 [0.37-0.42]	0.82 [0.79-0.85]	0.85 [0.81-0.86]	0.28 [0.27-0.29]	0.28 [0.27-0.28]
Striato-postcentral tract	0.41 [0.38-0.42]	0.39 [0.37-0.41]	0.77 [0.76-0.82]	0.81 [0.78-0.83]	0.29 [0.28-0.30]	0.28 [0.27-0.29]
Striato-precentral tract	0.41 [0.38-0.42]	0.39 [0.37-0.41]	0.75 [0.74-0.80]	0.79 [0.76-0.81]	0.30 [0.28-0.31]	0.28 [0.27-0.30]
Striato-prefrontal tract	0.37 [0.34-0.38]	0.34 [0.32-0.37]	0.80 [0.80-0.86]	0.84 [0.81-0.86]	0.27 [0.25-0.28]	0.26 [0.25-0.27]
Striato-premotor tract	0.37 [0.34-0.39]	0.34 [0.32-0.38]	0.74 [0.73-0.81]	0.79 [0.76-0.83]	0.29 [0.26-0.30]	0.27 [0.26-0.29]
Superior thalamic radiation	0.43 [0.42-0.47]	0.42 [0.41-0.45]	0.74 [0.72-0.77]	0.77 [0.74-0.78]	0.31 [0.29-0.32]	0.30 [0.29-0.31]
Thalamo-parietal tract	0.41 [0.39-0.43]	0.40 [0.38-0.42]	0.83 [0.80-0.88]	0.84 [0.83-0.88]	0.29 [0.27-0.29]	0.27 [0.27-0.29]
Thalamo-postcentral tract	0.44 [0.43-0.47]	0.44 [0.41-0.46]	0.77 [0.74-0.79]	0.79 [0.77-0.81]	0.31 [0.30-0.32]	0.30 [0.29-0.31]
Thalamo-precentral tract	0.44 [0.42-0.46]	0.42 [0.40-0.45]	0.72 [0.71-0.77]	0.77 [0.74-0.77]	0.31 [0.30-0.32]	0.30 [0.29-0.31]
Thalamo-prefrontal tract	0.39 [0.37-0.41]	0.37 [0.35-0.40]	0.81 [0.78-0.85]	0.83 [0.82-0.85]	0.28 [0.26-0.29]	0.26 [0.26-0.27]
Thalamo-premotor tract	0.41 [0.39-0.41]	0.38 [0.36-0.40]	0.75 [0.72-0.78]	0.79 [0.75-0.80]	0.29 [0.27-0.30]	0.28 [0.27-0.29]

Variables are listed as median [IQR]. P-values are without correction for multiple comparisons. The green box shows a significant difference ( $p < 0.05$ ) between patients with normal and impaired cognition.

## Appendix E. MEDIAN DIFFUSIVITY MEASURES PER TRACT GROUPED BY NEUROLOGICAL OUTCOME IN RIJNSTATE POPULATION

Table 7: Median [IQR] fractional anisotropy (FA), mean diffusivity (MD), and apparent fiber density (AFD) in 32 white matter tracts throughout the whole brain only in the Rijnstate population, grouped by neurological outcome (good or poor).

Metric	FA		MD (*10 <sup>-3</sup> )		AFD	
	Good (29)	Poor (20)	Good (29)	Poor (20)	Good (29)	Poor (20)
Neurological outcome						
Genu and body (corpus callosum)	0.42 [0.40-0.43]	0.42 [0.38-0.44]	0.95 [0.91-1.00]	0.97 [0.89-1.04]	0.26 [0.24-0.26]	0.26 [0.24-0.28]
Superior longitudinal fasciculus	0.38 [0.36-0.40]	0.36 [0.34-0.39]	0.78 [0.75-0.81]	0.77 [0.68-0.85]	0.28 [0.27-0.29]	0.29 [0.27-0.31]
Corticospinal tract	0.34 [0.33-0.36]	0.31 [0.31-0.35]	0.87 [0.85-0.88]	0.89 [0.82-0.94]	0.27 [0.26-0.28]	0.27 [0.25-0.29]
Thalamo-occipital tract	0.52 [0.50-0.54]	0.50 [0.48-0.53]	0.80 [0.75-0.82]	0.80 [0.76-0.84]	0.31 [0.29-0.32]	0.30 [0.28-0.32]
Uncinate fasciculus	0.41 [0.39-0.43]	0.40 [0.36-0.44]	0.89 [0.87-0.98]	0.90 [0.86-0.98]	0.27 [0.26-0.27]	0.27 [0.25-0.29]
Arcuate fascicle	0.37 [0.36-0.40]	0.36 [0.34-0.40]	0.78 [0.76-0.81]	0.78 [0.72-0.85]	0.28 [0.27-0.29]	0.29 [0.26-0.31]
Anterior thalamic radiation	0.34 [0.32-0.37]	0.32 [0.30-0.34]	0.87 [0.86-0.89]	0.90 [0.82-0.97]	0.25 [0.24-0.26]	0.26 [0.23-0.28]
Commissure anterior	0.30 [0.26-0.38]	0.29 [0.23-0.34]	0.91 [0.88-0.97]	0.93 [0.87-0.99]	0.22 [0.19-0.23]	0.22 [0.19-0.24]
Rostrum (Corpus Callosum)	0.42 [0.38-0.44]	0.40 [0.35-0.43]	0.91 [0.88-0.96]	0.92 [0.81-1.00]	0.23 [0.22-0.23]	0.25 [0.22-0.27]
Isthmus (Corpus Callosum)	0.45 [0.43-0.47]	0.45 [0.42-0.48]	0.93 [0.91-1.00]	0.94 [0.83-0.99]	0.27 [0.26-0.27]	0.27 [0.26-0.29]
Splenium (Corpus Callosum)	0.49 [0.46-0.51]	0.47 [0.43-0.53]	1.02 [0.98-1.07]	1.01 [0.91-1.10]	0.27 [0.26-0.28]	0.27 [0.25-0.30]
Cingulum	0.37 [0.36-0.40]	0.34 [0.32-0.39]	0.80 [0.77-0.83]	0.82 [0.76-0.89]	0.28 [0.27-0.28]	0.29 [0.26-0.31]
Fronto-pontine tract	0.46 [0.44-0.48]	0.44 [0.42-0.48]	0.80 [0.79-0.82]	0.73 [0.77-0.88]	0.28 [0.27-0.29]	0.28 [0.26-0.29]
Inferior occipito-frontal fascicle	0.40 [0.38-0.42]	0.37 [0.35-0.41]	0.88 [0.86-0.94]	0.89 [0.84-0.98]	0.27 [0.26-0.28]	0.28 [0.25-0.29]
Inferior longitudinal fasciculus	0.40 [0.39-0.42]	0.38 [0.35-0.43]	0.87 [0.85-0.91]	0.86 [0.79-0.95]	0.27 [0.26-0.28]	0.27 [0.25-0.29]
Middle cerebellar peduncle	0.47 [0.45-0.49]	0.43 [0.41-0.48]	0.79 [0.75-0.83]	0.82 [0.78-0.84]	0.31 [0.28-0.34]	0.29 [0.27-0.31]
Middle longitudinal fasciculus	0.37 [0.34-0.39]	0.35 [0.33-0.39]	0.84 [0.81-0.86]	0.83 [0.75-0.90]	0.28 [0.27-0.28]	0.28 [0.26-0.30]
Optic radiation	0.42 [0.40-0.43]	0.40 [0.36-0.44]	0.88 [0.86-0.96]	0.89 [0.85-0.98]	0.27 [0.26-0.27]	0.27 [0.25-0.29]
Parieto-occipital pontine	0.46 [0.43-0.48]	0.44 [0.42-0.48]	0.85 [0.83-0.87]	0.87 [0.80-0.92]	0.29 [0.28-0.29]	0.29 [0.27-0.30]
Superior cerebellar peduncle	0.42 [0.40-0.45]	0.40 [0.39-0.44]	0.90 [0.87-0.95]	0.91 [0.88-0.95]	0.30 [0.28-0.31]	0.29 [0.27-0.30]
Striato-fronto-orbital tract	0.33 [0.31-0.35]	0.30 [0.27-0.33]	0.87 [0.85-0.89]	0.89 [0.80-0.95]	0.24 [0.23-0.26]	0.26 [0.23-0.27]
Striato-occipital tract	0.42 [0.41-0.45]	0.40 [0.37-0.44]	0.88 [0.87-0.95]	0.88 [0.84-0.97]	0.28 [0.26-0.28]	0.28 [0.26-0.30]
Striato-parietal tract	0.39 [0.36-0.41]	0.36 [0.33-0.39]	0.85 [0.82-0.87]	0.85 [0.78-0.90]	0.28 [0.27-0.28]	0.28 [0.26-0.30]
Striato-postcentral tract	0.38 [0.36-0.41]	0.36 [0.32-0.39]	0.81 [0.78-0.84]	0.80 [0.75-0.85]	0.28 [0.27-0.29]	0.29 [0.27-0.31]
Striato-precentral tract	0.38 [0.37-0.41]	0.36 [0.33-0.39]	0.80 [0.77-0.81]	0.79 [0.74-0.84]	0.29 [0.28-0.29]	0.29 [0.27-0.31]
Striato-prefrontal tract	0.34 [0.32-0.36]	0.31 [0.29-0.35]	0.85 [0.82-0.87]	0.86 [0.79-0.94]	0.26 [0.25-0.27]	0.27 [0.24-0.29]
Striato-premotor tract	0.34 [0.32-0.37]	0.32 [0.30-0.35]	0.79 [0.77-0.84]	0.79 [0.75-0.87]	0.27 [0.26-0.28]	0.28 [0.25-0.30]
Superior thalamic radiation	0.41 [0.39-0.46]	0.41 [0.39-0.46]	0.77 [0.75-0.78]	0.77 [0.72-0.82]	0.30 [0.29-0.30]	0.30 [0.28-0.32]
Thalamo-parietal tract	0.40 [0.37-0.41]	0.38 [0.35-0.42]	0.86 [0.84-0.89]	0.86 [0.79-0.91]	0.28 [0.27-0.28]	0.28 [0.27-0.30]
Thalamo-postcentral tract	0.43 [0.40-0.46]	0.41 [0.39-0.44]	0.80 [0.77-0.82]	0.79 [0.74-0.83]	0.30 [0.29-0.31]	0.30 [0.28-0.32]
Thalamo-precentral tract	0.42 [0.40-0.44]	0.40 [0.38-0.44]	0.77 [0.74-0.77]	0.77 [0.72-0.81]	0.30 [0.29-0.31]	0.30 [0.28-0.32]
Thalamo-prefrontal tract	0.36 [0.35-0.39]	0.34 [0.32-0.37]	0.83 [0.82-0.86]	0.87 [0.80-0.92]	0.26 [0.26-0.27]	0.27 [0.25-0.29]
Thalamo-premotor tract	0.38 [0.36-0.40]	0.36 [0.34-0.39]	0.79 [0.75-0.81]	0.80 [0.75-0.84]	0.28 [0.27-0.28]	0.28 [0.26-0.30]

Variables are listed as median [IQR]. P-values are without correction for multiple comparisons. Green boxes show a significant difference between patients with good and poor neurological outcome. Light green indicates a p-value <0.05 and dark green a p-value <0.01.

## Appendix F. MEDIAN DIFFUSIVITY MEASURES PER TRACT GROUPED BY COGNITIVE PERFORMANCE IN RIJNSTATE POPULATION

Table 8: Median [IQR] fractional anisotropy (FA), mean diffusivity (MD), and apparent fiber density (AFD) in 32 white matter tracts throughout the whole brain only in the Rijnstate population, grouped by cognitive performance (normal or impaired).

Metric	FA		MD (*10 <sup>-3</sup> )		AFD	
	Normal (n=11)	Impaired (n=16)	Normal (n=11)	Impaired (n=16)	Normal (n=11)	Impaired (n=16)
<i>Neurological outcome</i>						
Genu and body (corpus callosum)	0.42 [0.41-0.44]	0.42 [0.40-0.43]	1.01 [0.91-1.04]	0.95 [0.93-1.00]	0.24 [0.24-0.27]	0.26 [0.25-0.26]
Superior longitudinal fasciculus	0.39 [0.38-0.39]	0.37 [0.36-0.40]	0.78 [0.74-0.80]	0.78 [0.76-0.81]	0.28 [0.27-0.29]	0.27 [0.27-0.28]
Corticospinal tract	0.35 [0.34-0.36]	0.34 [0.33-0.37]	0.87 [0.84-0.90]	0.87 [0.84-0.89]	0.27 [0.25-0.28]	0.28 [0.27-0.28]
Thalamo-occipital tract	0.52 [0.51-0.54]	0.51 [0.50-0.53]	0.81 [0.78-0.82]	0.78 [0.75-0.83]	0.30 [0.29-0.31]	0.30 [0.29-0.32]
Uncinate fasciculus	0.41 [0.39-0.43]	0.41 [0.38-0.42]	0.89 [0.87-0.99]	0.91 [0.87-0.94]	0.27 [0.25-0.27]	0.27 [0.26-0.28]
Arcuate fascicle	0.38 [0.37-0.40]	0.37 [0.35-0.39]	0.78 [0.74-0.81]	0.79 [0.76-0.81]	0.28 [0.28-0.29]	0.28 [0.27-0.29]
Anterior thalamic radiation	0.35 [0.31-0.37]	0.34 [0.32-0.36]	0.88 [0.85-0.93]	0.87 [0.87-0.89]	0.25 [0.24-0.27]	0.25 [0.24-0.26]
Commissure anterior	0.29 [0.27-0.33]	0.29 [0.21-0.37]	0.97 [0.88-0.10]	0.92 [0.60-0.95]	0.22 [0.20-0.23]	0.21 [0.14-0.23]
Rostrum (Corpus Callosum)	0.42 [0.39-0.43]	0.42 [0.38-0.44]	0.94 [0.90-0.99]	0.91 [0.89-0.96]	0.23 [0.22-0.25]	0.23 [0.23-0.24]
Isthmus (Corpus Callosum)	0.44 [0.44-0.46]	0.44 [0.43-0.46]	0.97 [0.92-0.10]	0.95 [0.91-0.10]	0.26 [0.26-0.27]	0.27 [0.26-0.27]
Splenium (Corpus Callosum)	0.49 [0.45-0.51]	0.48 [0.46-0.50]	0.10 [0.97-0.11]	0.10 [0.10-0.11]	0.26 [0.25-0.28]	0.27 [0.26-0.28]
Cingulum	0.38 [0.37-0.39]	0.37 [0.35-0.40]	0.80 [0.77-0.83]	0.81 [0.78-0.83]	0.28 [0.26-0.28]	0.28 [0.27-0.28]
Fronto-pontine tract	0.46 [0.45-0.47]	0.44 [0.43-0.47]	0.80 [0.78-0.85]	0.80 [0.77-0.84]	0.28 [0.27-0.29]	0.28 [0.27-0.29]
Inferior occipito-frontal fascicle	0.40 [0.38-0.42]	0.39 [0.38-0.42]	0.87 [0.86-0.94]	0.89 [0.86-0.93]	0.27 [0.26-0.28]	0.27 [0.26-0.28]
Inferior longitudinal fasciculus	0.41 [0.39-0.42]	0.40 [0.38-0.42]	0.86 [0.82-0.89]	0.87 [0.85-0.90]	0.26 [0.26-0.28]	0.27 [0.26-0.28]
Middle cerebellar peduncle	0.48 [0.44-0.49]	0.47 [0.46-0.49]	0.79 [0.79-0.82]	0.78 [0.74-0.84]	0.30 [0.28-0.84]	0.31 [0.29-0.34]
Middle longitudinal fasciculus	0.37 [0.35-0.37]	0.37 [0.34-0.38]	0.83 [0.80-0.88]	0.85 [0.82-0.87]	0.28 [0.27-0.28]	0.27 [0.27-0.28]
Optic radiation	0.41 [0.39-0.43]	0.42 [0.39-0.42]	0.89 [0.87-0.97]	0.89 [0.86-0.94]	0.27 [0.25-0.27]	0.27 [0.26-0.28]
Parieto-occipital pontine	0.46 [0.45-0.48]	0.46 [0.44-0.47]	0.86 [0.84-0.89]	0.85 [0.83-0.87]	0.29 [0.27-0.29]	0.28 [0.28-0.29]
Superior cerebellar peduncle	0.44 [0.42-0.45]	0.42 [0.40-0.43]	0.90 [0.85-0.93]	0.89 [0.86-0.96]	0.28 [0.28-0.31]	0.30 [0.28-0.31]
Striato-fronto-orbital tract	0.33 [0.32-0.34]	0.33 [0.30-0.36]	0.89 [0.85-0.93]	0.87 [0.85-0.88]	0.24 [0.22-0.26]	0.24 [0.23-0.26]
Striato-occipital tract	0.42 [0.40-0.45]	0.43 [0.40-0.44]	0.87 [0.87-0.95]	0.89 [0.86-0.94]	0.28 [0.27-0.28]	0.27 [0.27-0.28]
Striato-parietal tract	0.39 [0.38-0.41]	0.39 [0.36-0.40]	0.84 [0.82-0.88]	0.85 [0.82-0.87]	0.28 [0.26-0.28]	0.27 [0.27-0.28]
Striato-postcentral tract	0.39 [0.38-0.41]	0.38 [0.36-0.40]	0.81 [0.78-0.86]	0.81 [0.79-0.83]	0.29 [0.27-0.29]	0.28 [0.27-0.29]
Striato-precentral tract	0.39 [0.38-0.42]	0.38 [0.36-0.40]	0.79 [0.75-0.84]	0.80 [0.77-0.82]	0.29 [0.26-0.30]	0.28 [0.27-0.29]
Striato-prefrontal tract	0.34 [0.33-0.36]	0.33 [0.32-0.36]	0.85 [0.81-0.90]	0.85 [0.83-0.86]	0.25 [0.24-0.27]	0.25 [0.24-0.26]
Striato-premotor tract	0.35 [0.32-0.36]	0.33 [0.31-0.35]	0.79 [0.75-0.85]	0.81 [0.77-0.83]	0.26 [0.25-0.28]	0.26 [0.26-0.27]
Superior thalamic radiation	0.42 [0.41-0.45]	0.42 [0.40-0.44]	0.76 [0.75-0.80]	0.78 [0.74-0.78]	0.30 [0.28-0.30]	0.30 [0.29-0.30]
Thalamo-parietal tract	0.40 [0.39-0.42]	0.40 [0.37-0.41]	0.88 [0.83-0.92]	0.86 [0.84-0.89]	0.28 [0.26-0.29]	0.27 [0.27-0.28]
Thalamo-postcentral tract	0.43 [0.43-0.47]	0.43 [0.40-0.45]	0.77 [0.77-0.82]	0.80 [0.77-0.82]	0.30 [0.28-0.31]	0.29 [0.29-0.30]
Thalamo-precentral tract	0.42 [0.41-0.45]	0.42 [0.39-0.44]	0.75 [0.73-0.79]	0.77 [0.75-0.77]	0.30 [0.28-0.31]	0.29 [0.29-0.30]
Thalamo-prefrontal tract	0.38 [0.34-0.38]	0.36 [0.34-0.38]	0.84 [0.81-0.90]	0.83 [0.83-0.86]	0.26 [0.25-0.27]	0.26 [0.25-0.27]
Thalamo-premotor tract	0.39 [0.35-0.40]	0.37 [0.35-0.40]	0.77 [0.75-0.83]	0.79 [0.76-0.80]	0.27 [0.26-0.29]	0.27 [0.27-0.28]

Variables are listed as median [IQR]. P-values are without correction for multiple comparisons. Green boxes show a significant difference between patients with good and poor neurological outcome. Light green indicates a p-value <0.05 and dark green a p-value <0.01.